Thesis: Interannual Variations in the Earth's Radiative Budget and the General Circulation

Submitted by
James S. Ellis

Department of Atmospheric Science
Colorado State University
Fort Collins, Colorado

In partial fulfillment of the requirements for the Degree of Master of Science.
August 1972

Colorado State University

Department of Atmospheric Science

Paper No. 218

ATMOSPHERIC SCIENCE PAPER #218

THESIS

INTERANNUAL VARIATIONS IN THE EARTH'S RADIATIVE BUDGET AND THE GENERAL CIRCULATION

Submitted by

James S. Ellis

In partial fulfillment of the requirements

for the Degree of Master of Science

Colorado State University

Fort Collins, Colorado

August, 1972

INTERANNUAL VARIATIONS IN THE EARTH'S RADIATIVE BUDGET AND THE GENERAL CIRCULATION

The north-to-south gradient of net radiation, as determined from 35 months of satellite data, and parameters defining the intensity of the general circulation are brought together for the first time to investigate interrelationships in their year-to-year variations. An error analysis of the net radiation gradient is presented to attest to its validity. Parameterization of the atmosphere is accomplished through the zonal index, thermal wind and the eddy and zonal components of available potential and kinetic energies.

Statistical correlations indicate that, overall, interannual variations in the gradient of net radiation and the general circulation are out of phase by three months. However, for selected extreme variations, there are no apparent phase differences.

James Stephen Ellis
Atmospheric Science Department
Colorado State University
Fort Collins, Colorado 80521
August 1972

ACKNOWLEDGEMENTS

The author wishes to thank Dr. Thomas H. Vonder Haar for his patience and guidance and also Mr. Glenn W. Brier for his advice. Special thanks are extended to Charlene Polifka for computer programming, Vicki Brant for assistance in data reduction, Lyn Koch and Paula Brant for typing the manuscript, Dana Wooldridge for the graphic art, and to others, all of whom graciously gave of their time and skill.

The author is also indebted to the National Center for Atmospheric Research for a grant of their computing facility resources. This research was supported by NASA Grant No. NGR 06-002-12.

TABLE OF CONTENTS

	page
ABSTRACT	iii
ACKNOWLEDGEMENTS	iv
LIST OF FIGURES	vii
LIST OF TABLES	ix
1.0 Introduction	1
2.0 Radiation Data Analysis	3
2.1 Available Data	3
2.2 Net Radiation Gradient	5
2.2a Procedure	6
2.2b Gradient Analysis	7
2.3 Error Analysis	14
2.3a Bias Error	14
2.3b Other Error	18
2.4 Diurnal Effects	19
3.0 General Circulation and the Gradient of Net Radiation	23
3.1 Zonal Index	23
3.2 Thermal Wind	25
3.3 Energetics	26
3.3a Available Potential Energy	30
3.3b Kinetic Energy	34
3.4 Quantitative Comparison	36
4.0 Analysis of Results	43
4.1 Gradient and Circulation	43
4.1a Periodicity in Data	44
4.1b 3 Month Lag	48

page

4.2 Interhemisphere Comparison 51

4.3 Gradient and Cloudiness. 54

5.0 Summary and Conclusions 56

REFERENCES 58

LIST OF FIGURES

Figure		Page
1	Northern hemisphere monthly net radiation gradient (solid curve) and gradient of solar insolation (dashed curve) from 5N to 65N	8
2	Southern hemisphere monthly net radiation gradient (solid curve) and gradient of solar insolation (dashed curve) from 5S to 65S.	9
3	Northern hemisphere seasonal net radiation gradient (solid curve) and gradient of solar insolation (dashed curve) from 5N to 55N	11
4	Southern hemisphere seasonal net radiation gradient (solid curve) and gradient of solar insolation (dashed curve) from 5S to 55S	12
5	Net radiation bias error for infrared and albedo bias errors in the same direction.	16
6	Net radiation bias error for infrared and albedo bias errors in opposing directions	17
7	Diurnal variation in albedo and infrared radiation from TIROS 4 for April (after Vonder Haar and Hanson; see Vonder Haar, 1968)	20
8	Diurnal variation in albedo and infrared radiation from Nimbus 3 and ESSA 7 for April fitted with TIROS 4 profiles	21
9	Northern hemisphere monthly zonal index from 35N to 55N on a 700 mb surface (solid curve); mean monthly zonal index based upon a 9 year average (dashed curve)	24
10	Annual cycle of the net radiation gradient (ΔRN) and the thermal wind (V_T) based upon a 9 year average from 1963 to 1971.	27
11	Northern hemisphere thermal wind for the layer 1000 mb to 300 mb from 20N to 70N (solid curve); mean monthly thermal wind based upon a 9 year average (dashed curve).	28
12	Northern hemisphere zonal available potential energy in the mixed space-time domain for the layer 850 mb to 200 mb from 20N to 90N (solid curve); mean monthly zonal available potential energy based upon a 9 year average (dashed curve)	32
13	Northern hemisphere eddy available potential energy in the mixed space-time domain for the layer 850 mb to 200 mb from 20N to 90N (solid curve); mean monthly eddy available potential energy based upon a 9 year average (dashed curve)	33

		page
14	Northern hemisphere zonal kinetic energy in the mixed space-time domain for the layer 850 mb to 200 mb from 20N to 90N (solid curve); mean monthly zonal kinetic energy based on a 9 year average (dashed curve)	35
15	Northern hemisphere eddy kinetic energy in the mixed space-time domain for the later 850 mb to 200 mb from 20N to 90N (solid curve); mean monthly eddy kinetic energy based on a 9 year average (dashed curve)	37
16a	Correlation coefficients of interannual variations with the general circulation parameters leading (-months) and lagging (+months) the net radiation gradient. . . .	40
16b	Correlation coefficients of interannual variations with the general circulation parameters leading (-months) and lagging (+months) the net radiation gradient. . . .	41
17	Temporal distribution of the net radiation gradient with the annual cycle removed ($\Delta RN'$)	45
18	Spectrum analysis of general circulation parameters: smoothed spectrum (solid line), unsmoothed spectrum (dashed line)	47
19	Ocean storage curve for selected latitudes of the northern hemisphere (taken from data of Newell et al., 1969)	49
20	Correlation between interannual variations in net radiation gradient (black bars) and zonal available potential energy (light bars) with 3 months lag and no lag. . . .	50
21	Correlations between interannual variations in net radiation gradient (black bars) and zonal kinetic energy (light bars) with 3 months lag and no lag	52
22	Temporal comparison between interannual variations in the net radiation gradient of the northern hemisphere (solid line) and the southern hemisphere (dashed line)	53

LIST OF TABLES

Table		page
1	Available radiation data: TIROS 4 (T4), TIROS 7 (T7), Experimental (EX), Nimbus 2 (N2), Nimbus (N3), ESSA 3 (E3), ESSA 7 (E7) and ITOS 1 (I1).	4
2	Range of interannual variations in zonally average monthly net radiation at gradient latitudes (cal $cm^{-2}min^{-1}$). . .	13
3	Diurnal variations in net radiation (cal $cm^{-2}min^{-1}$). . .	19
4	Summary table of qualitative comparison between interannual variations in the net radiation gradient and the general circulation parameters	38

1.0 INTRODUCTION

Measurements from radiation sensors on earth orbiting satellites have allowed a study of the spatial distribution and the temporal variations in the radiative characteristics of the earth-atmosphere system. This information is fundamental to gaining a better understanding of the energy input to our oceanic and atmospheric circulation.

The net radiation budget (RN) is defined as the total incoming solar energy minus the sum of the outgoing scattered, reflected, and emitted energies which are measured at the top of the atmosphere.

The purpose of this report is to investigate the interannual variations in the north-to-south net radiation budget distribution and the relationship of these variations to the general circulation of the atmosphere.

The north-to-south net radiation budget distribution can be represented to a first approximation by the net radiation gradient (ΔRN), i.e., the north-to-south difference in the net radiation budget. Vonder Haar and Suomi (1969) first discussed the pole-to-equator ΔRN as a simple measure of the radiative forcing on the global circulation. The magnitude of ΔRN reflected the seasonal north-to-south migration of the sun's path on the earth but, more important were the interannual differences in the seasonal values of ΔRN (Vonder Haar and Suomi, 1971). These differences are most probably indirectly related to the year-to-year variations in the strength of the general circulation of the atmosphere through complex energy exchange mechanisms. This study is an attempt to detect related changes in the general circulation and to gain a better understanding of the feedback mechanisms.

The procedure will be to compute monthly values of ΔRN and then to compare them with general circulation parameters. Parameterization of the atmosphere has been accomplished to some degree by computing the zonal index, the thermal wind, and the potential and kinetic energies.

2.0 RADIATION DATA ANALYSIS

2.1 Available Data

The radiation data used in this study comprise the most complete set of reduced data available to data from radiation experiments on earth orbiting satellites, excluding only data which does not include both albedo and infrared measurements. The data are for 36 months and 5 additional seasons which together intermittently span 10 years from 1962 to 1971 (Table 1).

Discussion on the data reduction can be found in the following references: TIROS 4, TIROS 7, EXPERIMENTAL (Vonder Haar, 1968), Nimbus 2 (Raschke, 1968; Raschke and Bandeen, 1970), ESSA 3 preliminary results (MacDonald, 1969), Nimbus 3 (Raschke, et al., 1972), ITOS 1 preliminary results (Smith, 1972), and ESSA 7 (MacDonald, 1970 and 1972).

Data from 1962 through 1965 are the same as that used by Vonder Haar (1968) except for an adjustment in the solar constant from 2.00 cal cm^{-2} min^{-1} to 1.95 cal cm^{-2} min^{-1} (the solar constant used throughout this study). Half of the data (17 continuous months) are from the Wisconsin low resolution plate sensors flown on an experimental satellite. The remainder of the data were collected by the following sensors: medium resolution scanning radiometers on TIORS 7, Nimbus 2, and Nimbus 3; Wisconsin low resolution hemisphers on TIROS 4, and Wisconsin flat plate radiometers on ESSA 3, ESSA 7, and ITOS 1.

Five seasonal sets of data from the TIROS satellites were included to extend the data set back to 1962. Large gaps in the longitudinal

TABLE 1: Available radiation data: TIROS 4 (T4), TIROS 7 (T7), Experimental (EX), Nimbus 2 (N2), Nimbus 3 (N3), ESSA 3 (E3), ESSA 7 (E7) and ITOS 1 (I1).

	Year										
Months	1962	1963	1964	1965	1966	1967	1968	1969	1970	1971	No.
J				EX				E7	N3		3
F				EX				E7			2
M				EX				E7			2
A				EX				N3,E7			2
M				EX	N2			N3		I1	4
J				EX	N2			N3			3
J			EX	EX	N2			N3			4
A			EX	EX				N3			3
S			EX	EX							2
O			EX	EX			E7	N3			4
N			EX	EX			E7				3
D			EX		E3		E7				3
Seasons											
DJF		T7	EX		E3		E7	N3			
MAM	T4		T7	EX				E7,N3			
JJA		T7	EX	EX	N2			N3			
SON		T7	EX	EX			E7	N3			

NOTE: The DJF season is assigned the year of the respective December.

average limited the temporal resolution to seasons for complete longitudinal coverage.

2.2 Net Radiation Gradient

The net radiation gradient (ΔRN) is the north-to-south difference in the zonally averaged (latitudinal average) net radiation budget.

The net radiation budget (RN) at the top of a column extending from the surface to the top of the atmosphere (30 km) is defined precisely as:

$$RN = I_o (1 - A) - RL \tag{1}$$

where:

I_o = the solar irradiance on the top of the column determined by the solar constant 1.95 cal cm^{-2} min^{-1}.

A = the albedo - the ratio of outgoing scattered and reflected solar flux at the top of the column to I_o.

RL = the outgoing longwave radiation (emitted radiation) at the top of the column.

Each term of Eq. (1) is a function of both space and time.

The net radiation gradient was taken between latitudes 5^o and 65^o for the monthly data:

$$\Delta RN = RN_5 - RN_{65} \tag{2}$$

and between 5^o and 55^o latitudes for the seasonal data:

$$\Delta RN = RN_5 - RN_{55} \tag{3}$$

2.2a Procedure

Data prior to 1966 were gridded every 10^{o} latitude and 10^{o} longitude from 85^{o} north latitude to 85^{o} south latitude. The higher resolution data after 1965 were averaged to obtain the same gridding. Net radiation was computed at each grid point using the albedo, long-wave radiation, and solar insolation components. The net radiation gradient was computed from the zonally averaged net radiation budget for each data set.

Equation (2) was used to compute the net radiation gradient from the monthly data sets. The equatorward limit was selected at 5 degrees rather than the equator since it required no interpolation on the basic grid; interpolation at the equator would have required averaging over the zone 5^{o}N to 5^{o}S, where intertropical convergence zone migrates north and south during the course of a year.

The poleward limit was set at 65^{o} rather than 85^{o} because of the data coverage; ten monthly data sets had no data at 85^{o}N, however, only four data sets had missing data at 65^{o}N. Of these four sets, three had data both north and south of 65^{o}N (October 1964, October 1965, and February 1965). The net radiation at 65^{o}N could not be evaluated directly on these three occasions because the reflected energy was near the noise level of the signal. These three points were therefore, indirectly evaluated by interpolation using meridional profiles of the same months for other years. The zonally averaged net radiation 65^{o}N for the fourth data set (September 1964) was extrapolated using the meridional profile for September 1965. Similarly, for the gradient in the southern hemisphere, three August values were interpolated and June 1966 value was extrapolated to 65^{o}S.

Equation (3) was used to compute the net radiation gradient for the seasonal data. Since the TIROS data did not extend poleward of 55^{o}N and 55^{o}S latitude, the gradient was taken across the 55^{o} to 5^{o} latitude band. In addition, all monthly data were averaged into seasons so that a gradient comparison could be made.

2.2b Gradient Analysis

Monthly net radiation gradients (ΔRN) are presented in Figures 1 and 2 for the northern and southern hemispheres, respectively. The continuous solid curve traces the monthly mean gradient to show the intermonthly change in the gradient. The vertical lines with the horizontal bars followed by the year show the interannual variation in the monthly gradients. The continuous dashed curve traces the monthly gradient of incoming solar insolation (ΔI_o) taken over the same latitude belt. (Note that the scale of ΔI_o - to the right of the graph - is different than the scale of ΔRN).

The net radiation gradient declines less rapidly from spring to summer than it rises from summer to fall - apparent in both hemispheres. This is attributed to higher surface and atmospheric temperatures during fall in the poleward latitudes. Smaller longwave radiative loss in the poleward latitudes and smaller net radiative gain near the equator at winter solstice appears in both hemispheres as a sharp drop in the gradient - December in the northern and June in the southern. The rise from December to January in the northern hemispheres is probably due to the large gradient in the January 1970 Nimbus 3 data which was not available in December 1969, and is thus a consequence of the data set.

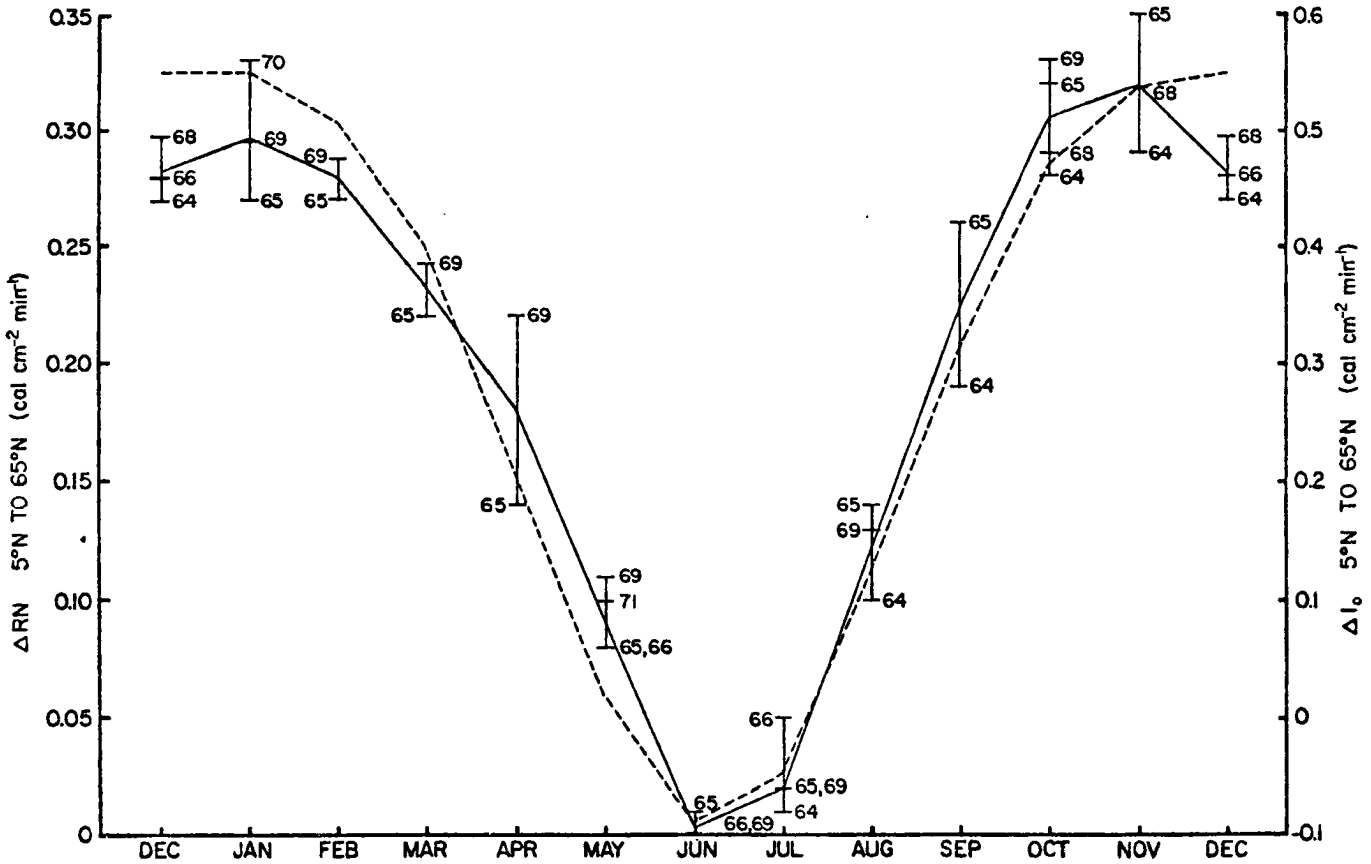

FIGURE 1. Northern hemisphere monthly net radiation gradient (solid curve) and gradient of solar insolation (dashed curve) from 5N to 65N.

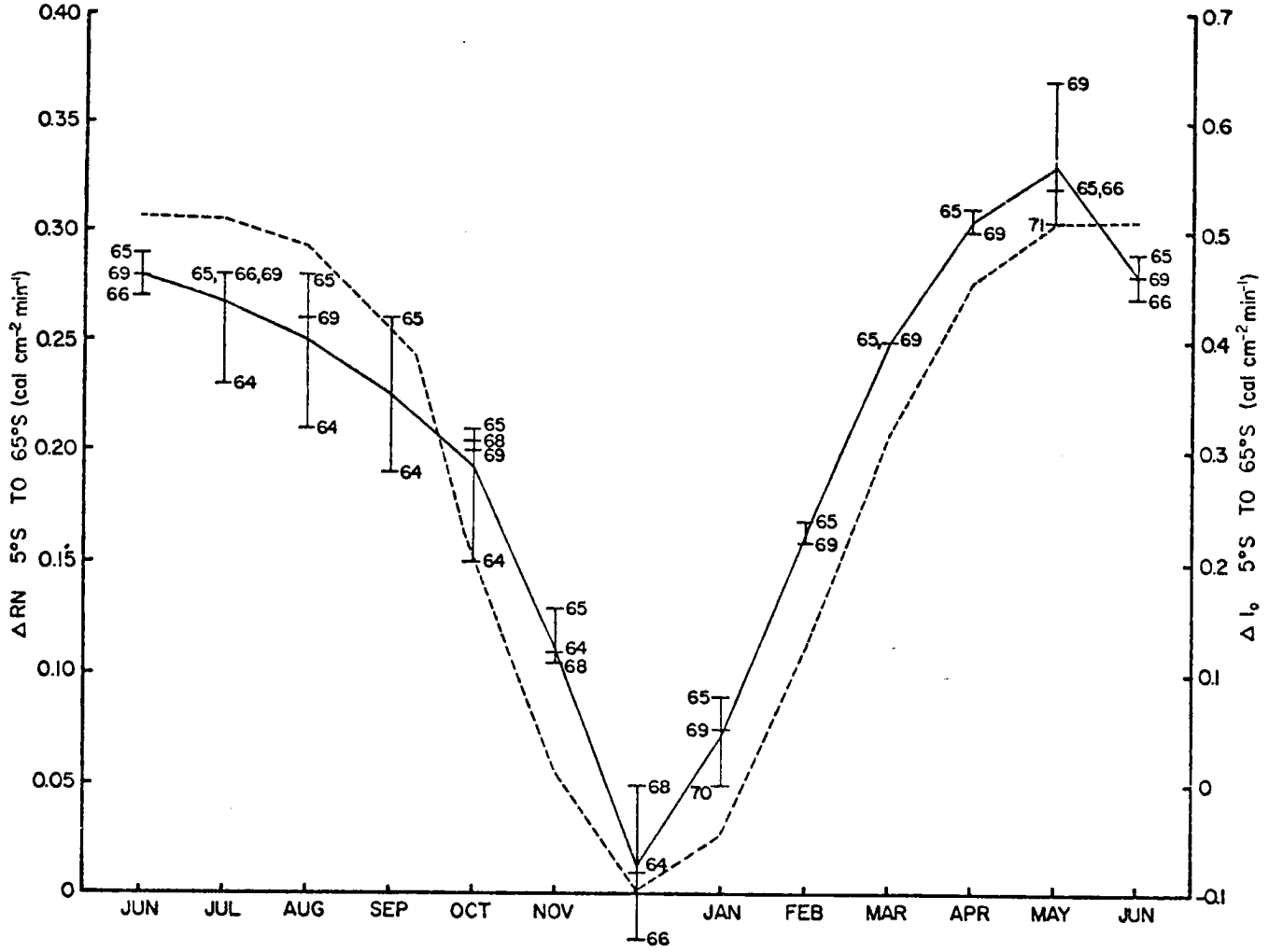

FIGURE 2. Southern hemisphere monthly net radiation gradient (solid curve) and gradient of solar insolation (dashed curve) from 5S to 65S.

Seasonal gradients appear in Figures 3 and 4 for the northern and southern hemispheres, respectively. A striking feature is the extremely sharp rise from summer to fall as compared to the moderate decline from spring to summer. This feature results primarily from the way the seasons are defined; the solstices and equinoxes do not fall in the center of the seasons but near the end of the first month in each season. Had the seasons been so defined to be centered on the equinoxes and solstices, then the profiles would have been near symmetrical except for a slight assymmetry as noted in the monthly profiles.

In both hemispheres the net radiation gradient is in phase with the gradient of solar insolation on both monthly and seasonal time scales. This does not exclude a phase shift for time scales less than a month. In addition, quite large year-to-year variations exist in the monthly and seasonal net radiation gradient - the primary concern of this study.

The range in the interannual variations in ΔRN and in RN at gradient latitudes are shown in Table 2. The range in the monthly RN variations is larger at 65N than at 5N latitudes and larger at 5S than at 65S latitudes. On the whole, the range is less at 65S than at 65N and less at 5N than at 5S. These relationships become most apparent by considering the average range for each which is also shown in the table. Therefore, the net radiation gradient is affected most by variations in net radiation at 65N for the northern hemisphere and at 5S for the southern hemisphere.

The next step is to establish through an error analysis that such variations in both ΔRN and RN are real and not data error.

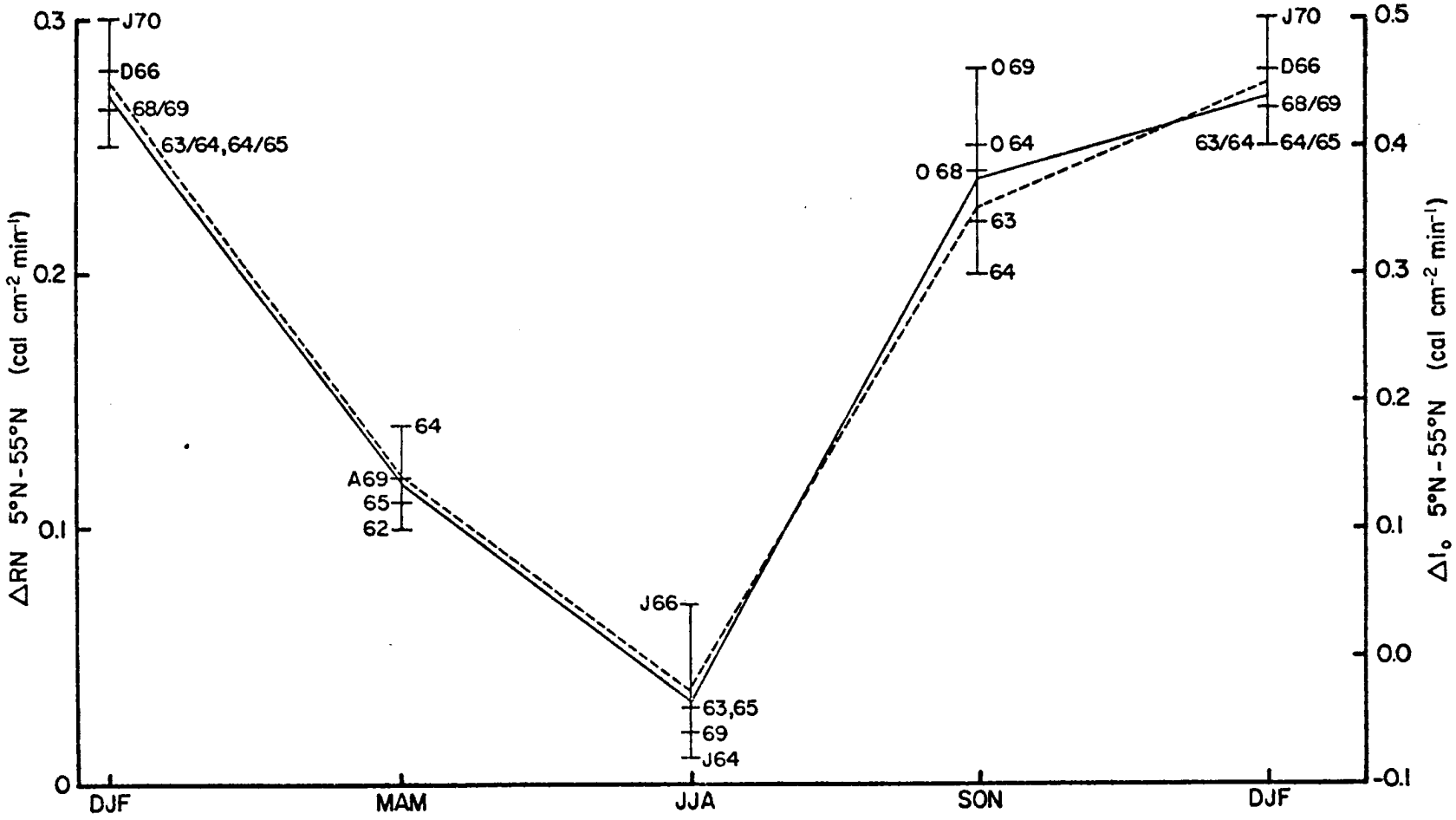

FIGURE 3. Northern hemisphere seasonal net radiation gradient (solid curve) and gradient of solar insolation (dashed curve) from 5N to 55N.

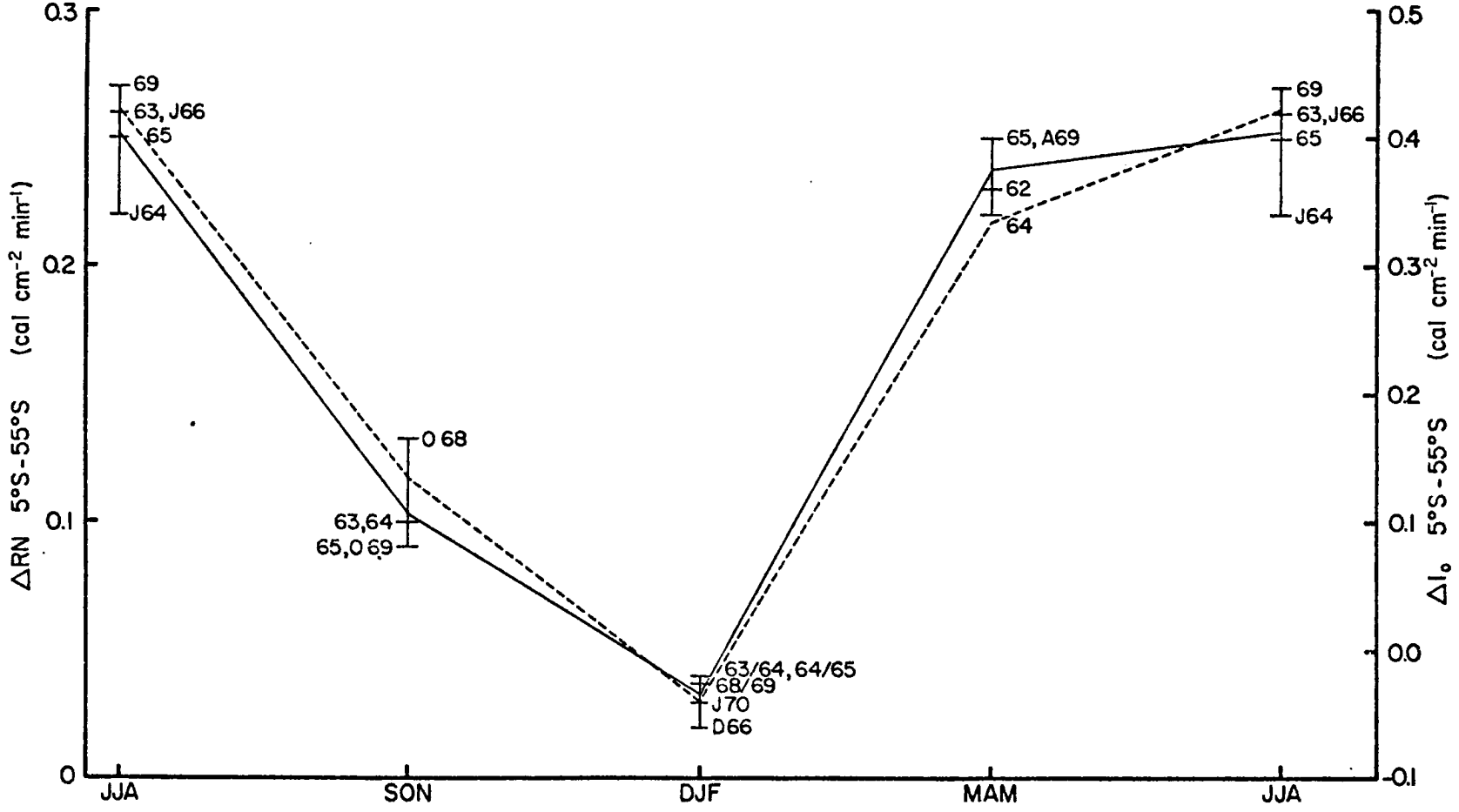

FIGURE 4. Southern hemisphere seasonal net radiation gradient (solid curve) and gradient of solar insolation (dashed curve) from 5S to 55S.

TABLE 2: Measured range of interannual variations in zonally averaged monthly net radiation at gradient latitudes (cal cm^{-2} min^{-1}). (see TABLE 1 for sample size).

Months	Northern Hemipshere			Southern Hemisphere		
	5N	65N	ΔRN_{5-65}	5S	65S	ΔRN_{5-65}
JAN	.03	.05	.06	.04	.06	.04
FEB	.02	.04	.02	.02	.01	.01
MAR	.03	.06	.02	.04	.04	.00
APR	.03	.10	.08	.06	.03	.03
MAY	.08	.10	.03	.09	.08	.06
JUN	.05	.04	.01	.05	.04	.02
JUL	.04	.06	.06	.05	.06	.05
AUG	.05	.04	.04	.05	.05	.07
SEP	.02	.05	.07	.04	.03	.07
OCT	.02	.04	.05	.03	.05	.06
NOV	.02	.05	.06	.02	.01	.03
DEC	.03	.05	.03	.07	.00	.06
AVG	.035	.057	.044	.047	.038	.042

2.3 Error Analysis

The type of error which can occur in data measurement and reduction are bias and random errors.

2.3a Bias Error

Vonder Haar (1968) thoroughly discussed the bias errors in the data prior to 1966. He established a most probable absolute error of ± 1.0 percent and ± 0.01 cal cm^{-2} min^{-1} in the albedo and longwave components, respectively. (These are equivalent to relative error of 3 to 5 percent.)

The total relative bias error in the same components from the Nimbus 3 satellite has been estimated to be near 5 percent (Raschke, et al., 1972). An error discussion by MacDonald (1970) would place bias error for ESSA 3 and ESSA 7 within the same limits.

Detailed discussion on the magnitude of bias error in the Nimbus 2 and ITOS 1 data are not available. Indication from Raschke, et al. (1970) is that the error in the Nimbus 2 data may be near or within the 5 percent estimated for Nimbus 3. Bias error in the preliminary data from ITOS 1 are presumed to be within the same 5 percent level.

The maximum probable bias error has therefore been set at 5 percent for the albedo and longwave components.

The total bias error in the net radiation gradient can now be determined. Differentiating Eq. (2) we get:

$$d(\Delta RN) = d\,RN_5 - d\,RN_{65} \tag{4}$$

Substituting from Eq. (1) and assuming that the solar constant is known exactly we get:

$$d(\Delta RN) = (I_o dA)_{65} - (I_o dA)_5 + dRL_{65} - dRL_5 \qquad (5)$$

We see that Eq. (5) is dependent upon the incoming solar insolation, a function of latitude and time, and the direction and magnitude of the bias error in albedo and longwave radiation.

There is no reason to suspect a sign change in dA or dRL with latitude so that dA will have the same sign at 5^o as at 65^o latitude and, similarly, for dRL. However, the error in albedo can be in the same or opposite direction of the error in longwave radiation. Eq. (5) has been used to calculate the bias error in the net radiation gradient for different months of the year with a ± 5 percent bias in each component. Actual data at both 5^oN and 65^oN were used in the computation.

The shaded area in Fig. 5 shows the monthly range in the net radiation gradient error when dA and dRL are of the same sign; a maximum of ± 0.014 cal cm^{-2} min^{-1} occurs in the winter months which is reduced to a range from zero to ± 0.004 cal cm^{-2} min^{-1} in the late spring and summer months. The other curves in the same figure show the bias error in the individual net radiation budgets at 5^oN and 65^oN. The bias at 5^oN is relatively unchanging throughout the year. The bias at 65^oN goes from a minimum during winter to a maximum during summer months.

Figure 6 shows the bias error in the gradient and component radiation budgets when dA and dRL have opposing signs. The maximum bias in this case is ± 0.010 cal cm^{-2} min^{-1} which occurs in spring to early summer. A minimum of ± 0.02 cal cm^{-2} min^{-1} occurs in the winter months. The smallest overall bias error exists in this case.

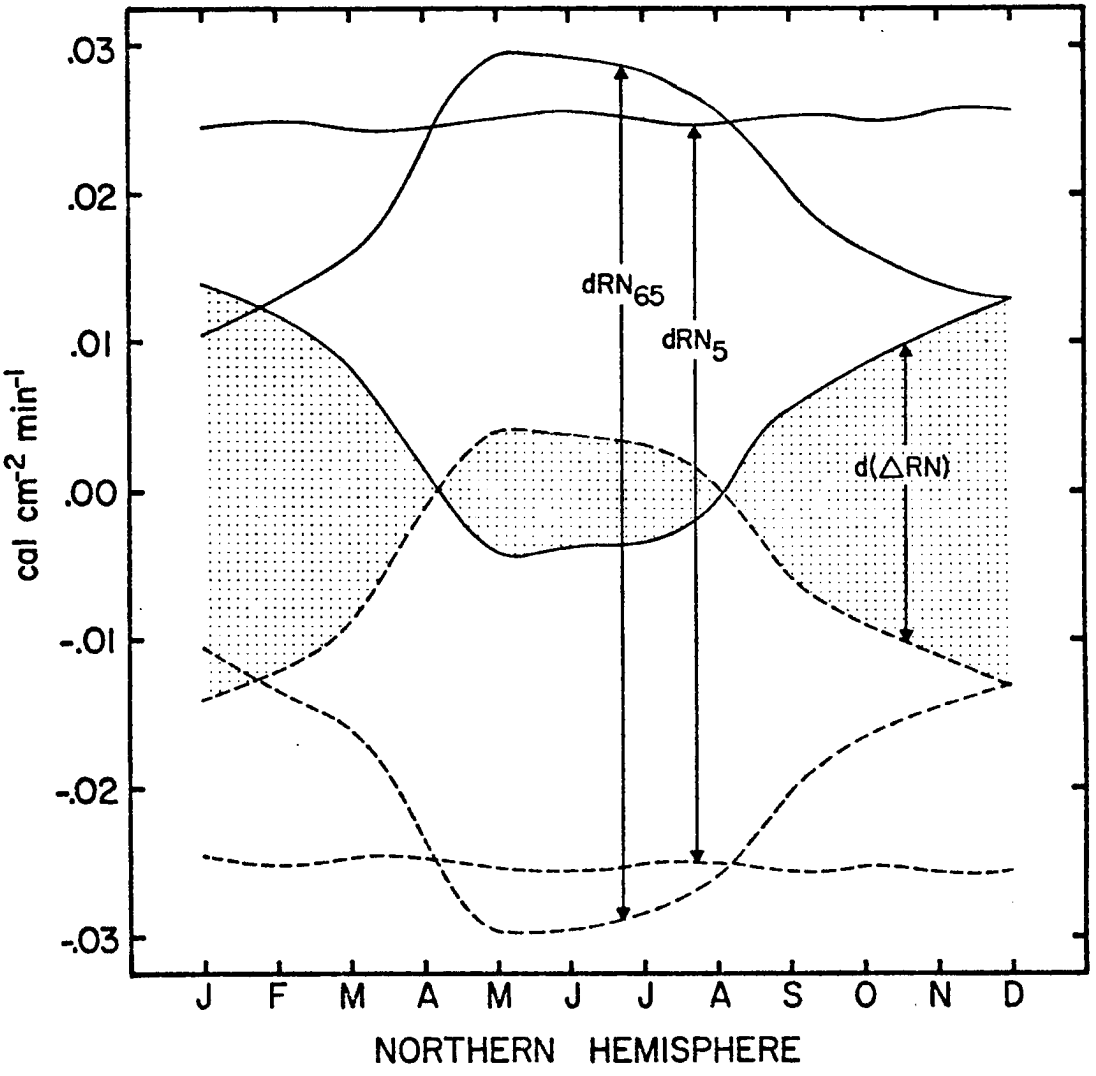

FIGURE 5. Net radiation bias error for infrared and albedo bias errors in the same direction.

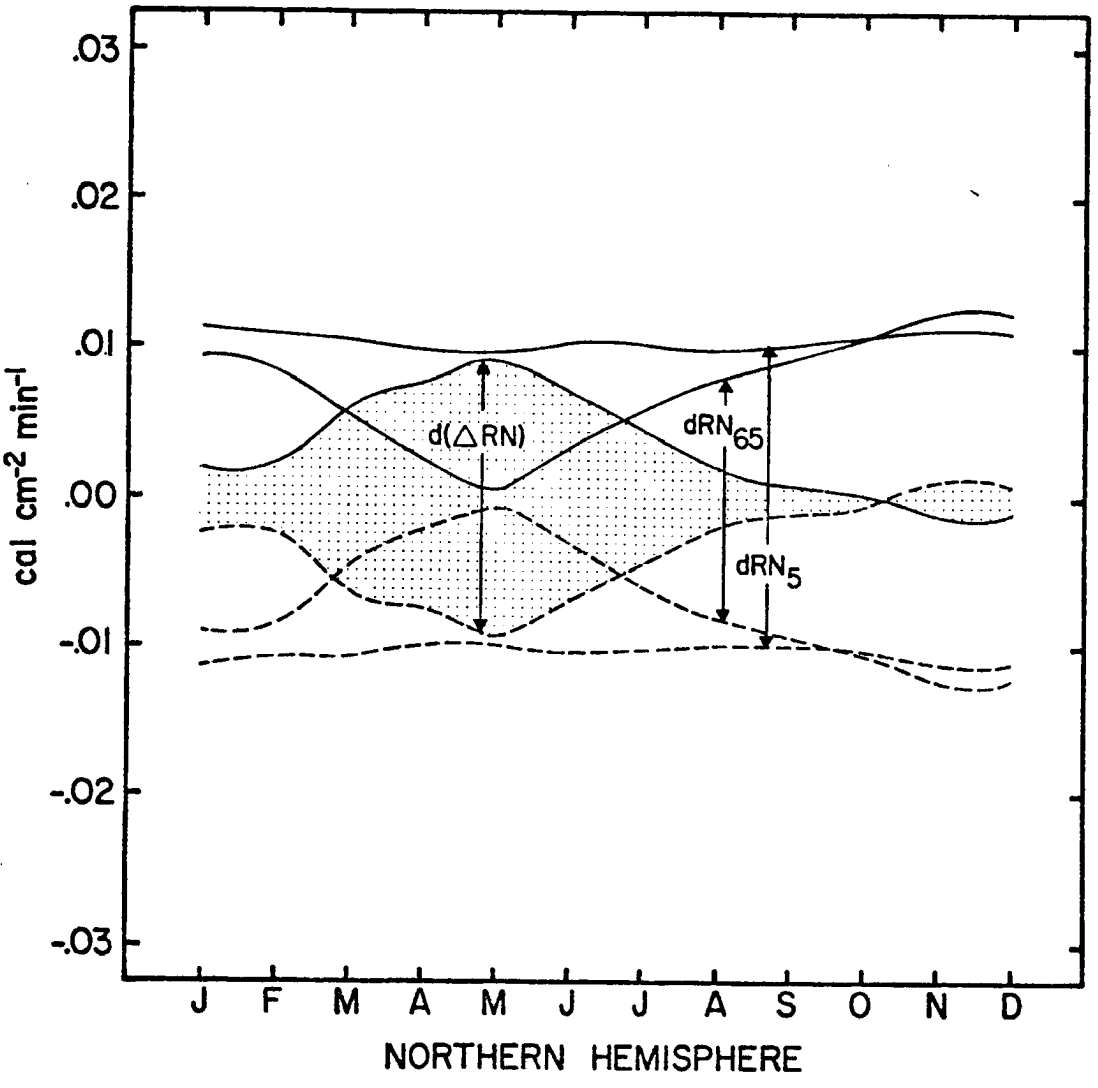

FIGURE 6. Net radiation bias error for infrared and albedo bias errors in opposing directions.

Previously, investigators have shown that dA and dRL are of opposite sign on the low resolution infrared radiometers on the experimental satellites. Thus, the bias error in the latter case applies to more than 75 percent of the data set.

Raschke, et. al. (1972) showed by use of a different reflectance model for reduction of Nimbus 3 data that the albedos over snow and ice (A > 50%) were overestimated by as much as 15 percent by the reduction model applied to Nimbus 2. Overestimates by such a magnitude would show up as a positive bias error in the net radiation gradient for that data because of the large ice field in the polar regions. Such error is minimized in the winter months when the solar insolation is small and maximized in the summer months when the solar insolation is at its greatest. However, from late spring to middle fall the sensor sees very little ice at 65^{o}. Thus, this bias falls within the previously computed bias error for the gradient.

2.3b Other Error

Error induced by uncertainty of the exact value of the solar constant affects each gradient equally. Hence, it does not change the relative interannual variation in the net radiation gradient and, therefore, can be neglected.

It is the opinion of this author that all random errors in time and space have been eliminated by using zonally averaged monthly mean and seasonally mean data.

2.4 Diurnal Effects

Earlier estimates of the diurnal variation in albedo and longwave radiation were made by Vonder Haar and Hanson (see Vonder Haar, 1968) for spring 1962, TIROS 4 data (Fig. 7). These preliminary results were compared to Nimbus 3 and ESSA 7 data from April 1969 which have approximate equator crossing times of 1130 and 1430 local, respectively (Fig. 8).

The absolute values in TIROS 4 albedo profiles had to be adjusted downwards by 5 to 8 percent to fit the new data. A profile at $65^{o}N$ was also estimated from the new data. A good fit exists between the new data and the preliminary albedo profiles depicting diurnal variation. We see that the albedo drops from early morning to mid-morning and then rises into the afternoon at all latitudes.

The longwave data did not fit the preliminary longwave profiles nearly as well as the albedo data except at $5^{o}N$ where a precise fit is again found. We see that a general decrease occurs in the longwave loss from early morning to afternoon.

The diurnal effect on the net radiation gradient for Nimbus 3 and ESSA 7 data in the month of April 1969 is shown in Table 3.

TABLE 3: Diurnal variations in net radiation (cal cm^{-2} min^{-1}) measured during April 1969

SATELLITE	NET RADIATION BUDGET		GRADIENT
	$5^{o}N$	$65^{o}N$	
NIMBUS 3	0.12	-0.10	0.22
ESSA 7	0.10	-0.06	0.16

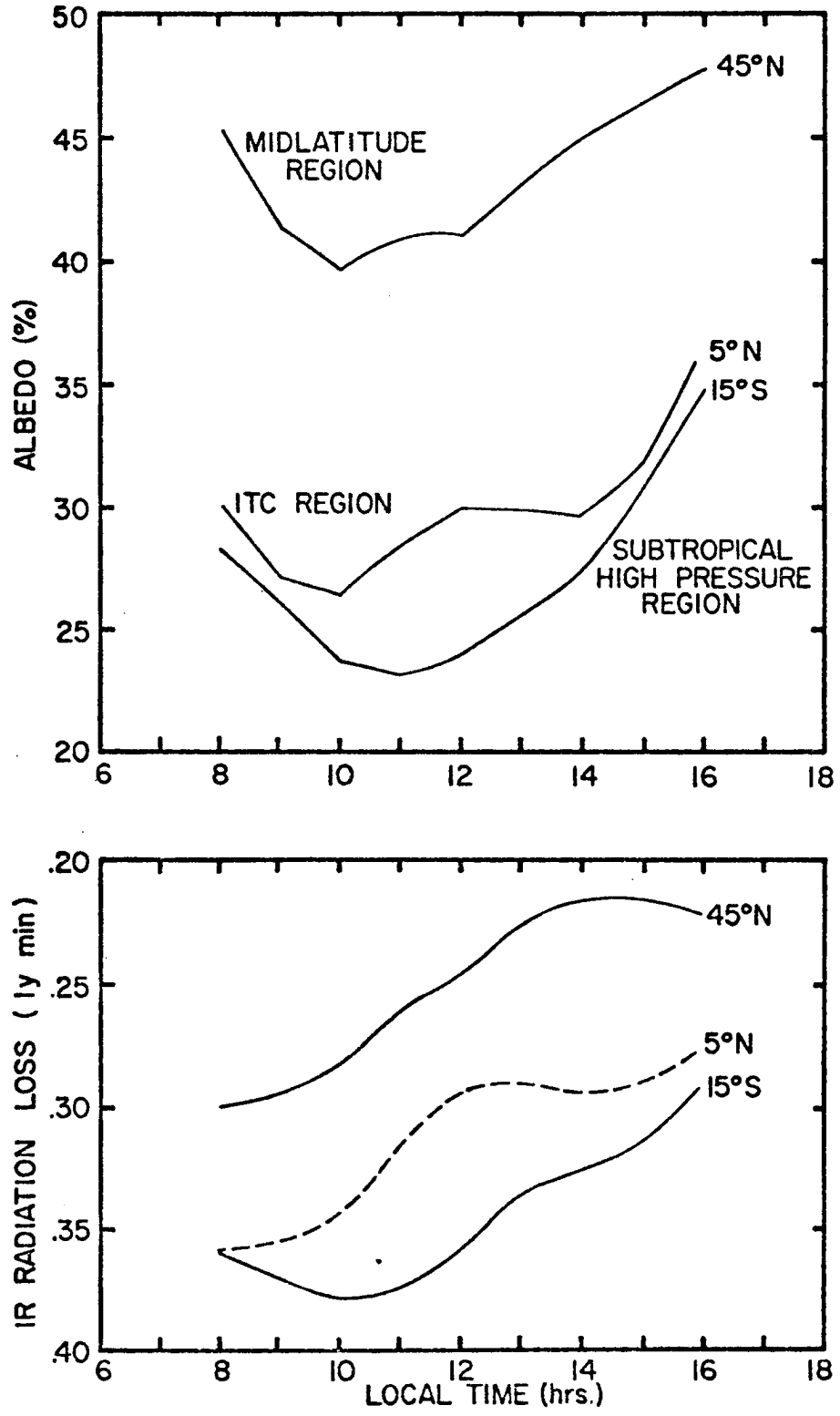

FIGURE 7. Diurnal variation in albedo and infrared radiation from TIROS 4 for April (after Vonder Haar and Hanson; see Vonder Haar, 1968).

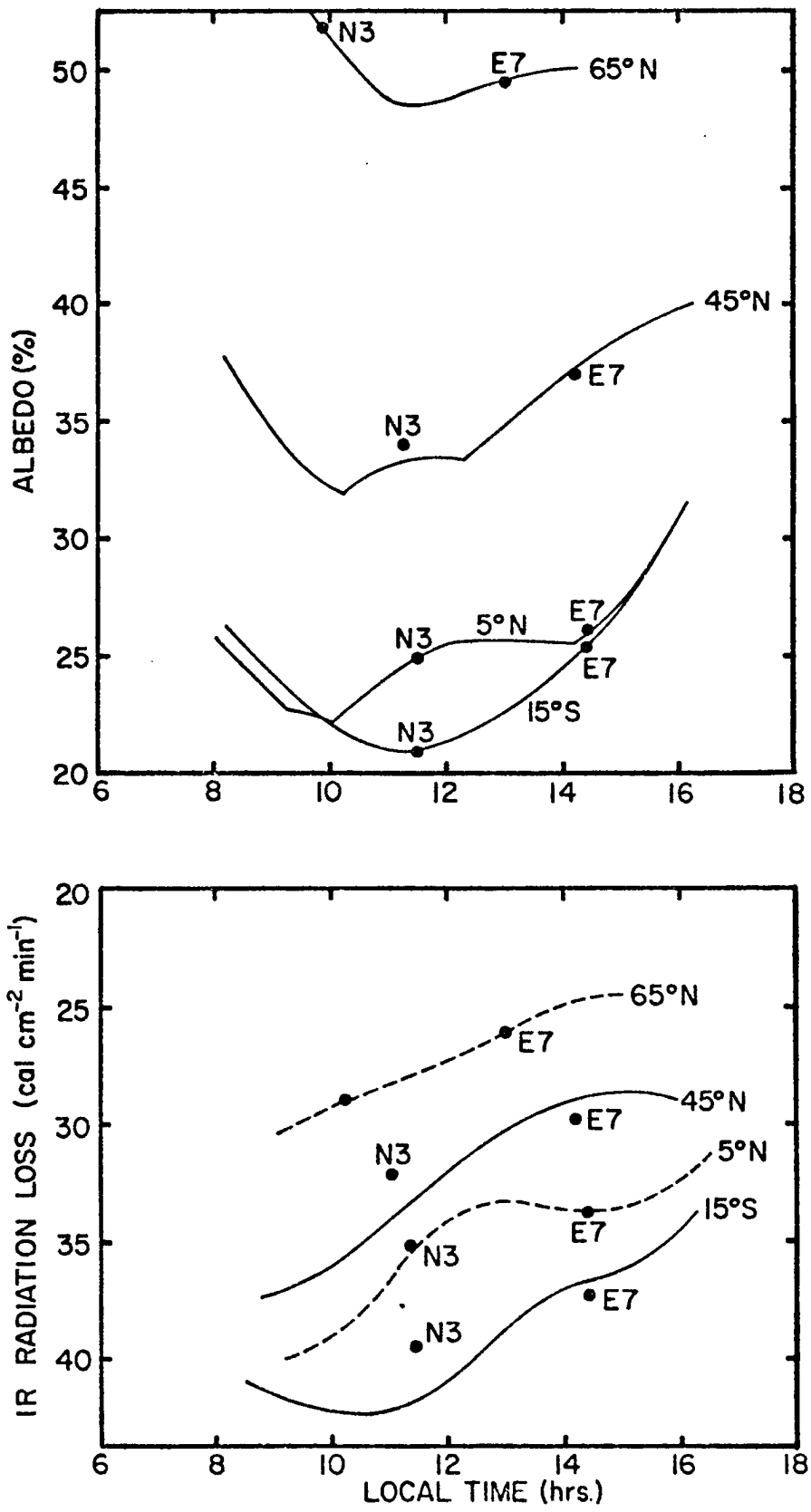

FIGURE 8. Diurnal variation in albedo and infrared radiation from Nimbus 3 and ESSA 7 for April fitted with TIROS 4 profiles.

The gradient near noon for Nimbus 3 data is 0.22 cal cm^{-2} min^{-1}. The gradient drops from near noon to afternoon to the ESSA 7 value of 0.16 cal cm^{-2} min^{-1}. This change of 0.06 cal cm^{-2} min^{-1} is well beyond the bias error which was computed to be 0.007 cal cm^{-2} min^{-1} for the month of April.

No adjustment have been made to the data in this study for the diurnal variation since the magnitude of its influence is not known for the other months of the year; it is certainly a function of the time of day, season and satellite orbital characteristics. Eventually the diurnal change will be measured for all seasons by experiments on geosynchronous satellites which have the capability to sample at all local times. One will then be able to adjust all of this earlier data for diurnal effects to get average daily radiation parameters and, hence, the gradient.

For the purpose of the study we will proceed with the knowledge that the net radiation gradient decreases from near noon to afternoon.

3.0 GENERAL CIRCULATION AND THE GRADIENT OF NET RADIATION

The intensity of the general circulation can be most quantitatively observed by parameterization of the atmosphere. Parameters selected for describing the atmosphere are: the zonal index, thermal wind, available potential energy, and kinetic energy. Each parameter was computed for each month of the 9 year period from January 1963 through October, 1971. Data for the computations were taken from the daily objective analysis of the National Meteorological Center (NMC).

3.1 Zonal Index

The zonal index (ZI) is the west-to-east component of the geostrophic wind taken across the 35^{o}N to 55^{o}N latitude band on a 700 mb surface. It has been described as a very stable index since its analysis over 20 years indicates typical fluctuations on the order of $\pm$5 percent (Kutzbach et al., 1968). Therefore, small changes in the index may infer significant changes in the general circulation.

Namias (1950) suggests that the zonal index is more of an indicator of the organization of the tropospheric circulation than a measure of its strength. The organization of the general circulation is indicated by low index (blocking patterns) and high index (zonal flow).

The zonal index shows the expected seasonal trend over the 9 year period (Figure 9). The dashed line represents the 9 year monthly averages and does not change from year to year. An interesting feature is the sharp decline in the index for February 1968 - low index. Examination of the tropospheric winds revealed the maximum winds to be above normal in strength but south of their normal position. Within the 35^{o}N to 55^{o}N latitude band the winds were more meridional than normal

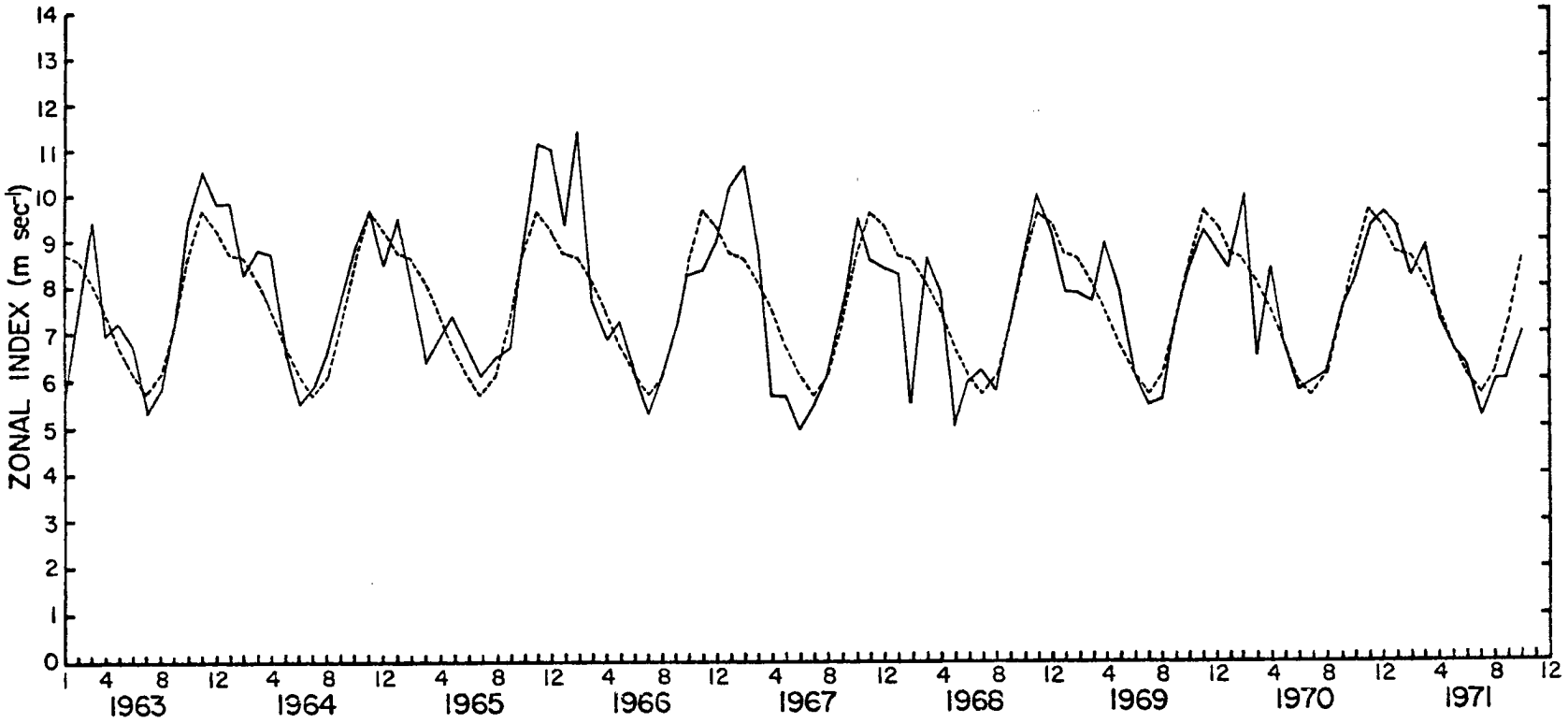

FIGURE 9. Northern hemisphere monthly zonal index from 35N to 55N on a 700 mb surface (solid curve); mean monthly zonal index based upon a 9 year average (dashed curve).

due to amplified troughs and ridges. The foregoing discussion points out that the index is not a good descriptor of the general circulation strength but may be, to a first approximation, a quantitative measure of the organization of the mid-latitude general circulation.

A notable feature is the above normal index for November, 1965 through February, 1966; it is approximately 20% higher than the mean indicating strong zonal flow. Other departures that may be significant are positive departures in winters 1963/64 and 1966/67 and negative departures in winter 1967/68 and spring to summer 1967.

A qualitative look at the net radiation gradient shows significantly stronger gradients in September through November 1965 than in the same months of 1964 (see Figure 1). However, the gradient and index may be inversely and neutrally related in winter 1963/64 and December 1966, respectively.

Also of interest is the November maximum in the mean zonal index profile which also appears in the mean net radiation gradient profile.

3.2 Thermal Wind

The thermal wind is defined as:

$$V_T = -\frac{g}{f}\frac{\partial}{\partial y}(\Delta Z)$$

where g is the acceleration due to gravity, f is the Coriolis parameter, $\frac{\partial}{\partial y}$ the north-to-south gradient from $20^{o}N$ to $70^{o}N$, and ΔZ the thickness of the 1000 to 300 mb layer.

The thermal wind was selected as a parameter since the north-to-south thermal gradient, implicit in the thermal wind, is indirectly

related to the north-to-south difference in radiative energy. This indirect relationship evolves primarily from diabatic heating of the atmosphere through latent and sensible heat transfer from a radiatively heated or cooled earth's surface. Figure 10 shows that the thermal wind lags the net radiation gradient by 4 to 6 weeks, an apparent indirect relationship.

One would hope to see a relationship between the interannual variations of the net radiation gradient and the thermal wind since the two appear to be related on a month to month basis. Examination of the thermal wind (V_T) over the nine year period (see Fig. 11) reveals significant positive anomalies in the following periods: November 1965 through February 1966, July 1966, January and February 1967, March 1969, April 1970, and January and July 1971. Significant negative anomalies appear in winters 1963/64 and 1967/68. The periods for which the net radiation gradient are available (winter 1963/64, November and December 1965, July 1966, and March 1969) have anomalies in the gradient with the same sign as the anomalies in the thermal wind (see Figure 1).

Of course one can start with a gradient anomaly and look for a corresponding anomaly in the thermal wind. Large positive anomalies in the gradient for April 1969 and January 1970 are not reflected in the thermal wind.

3.3 Energetics

Interannual changes in the net radiation gradient not reflected in the intensity of the general circulation may, however, cause the atmosphere to operate in a different mode. By computing available

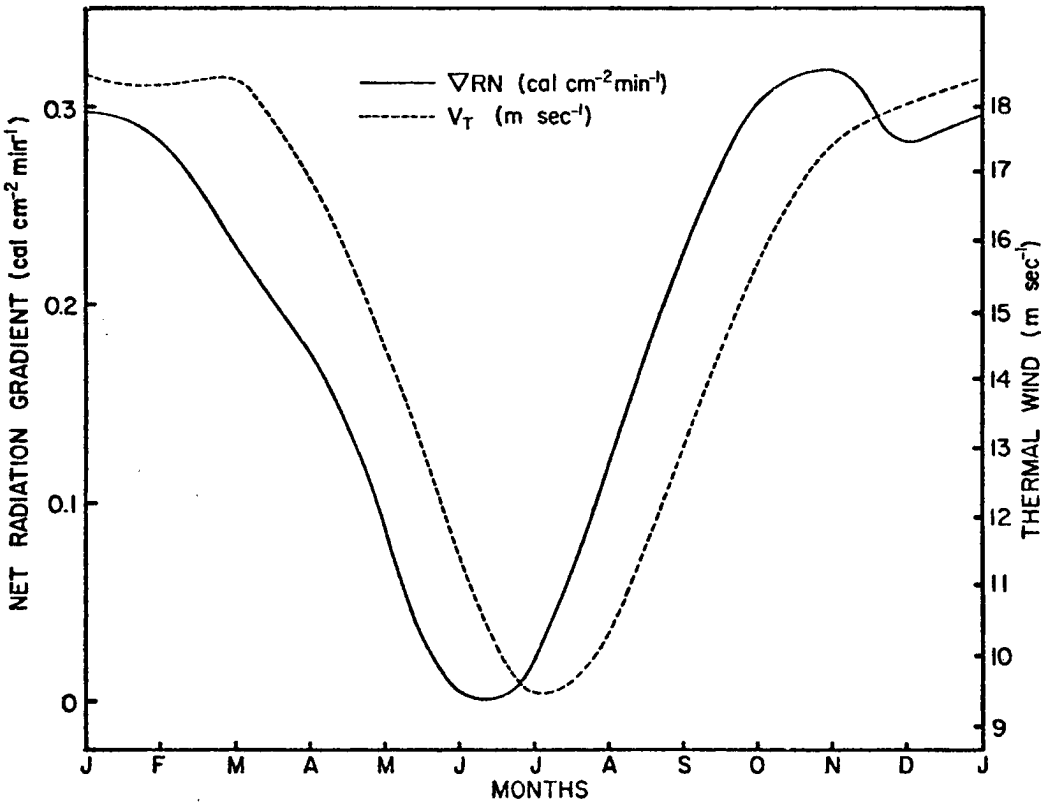

FIGURE 10. Annual cycle of the net radiation gradient (ΔRN) and the thermal wind (V_T) based on a 9 year average from 1963 to 1971.

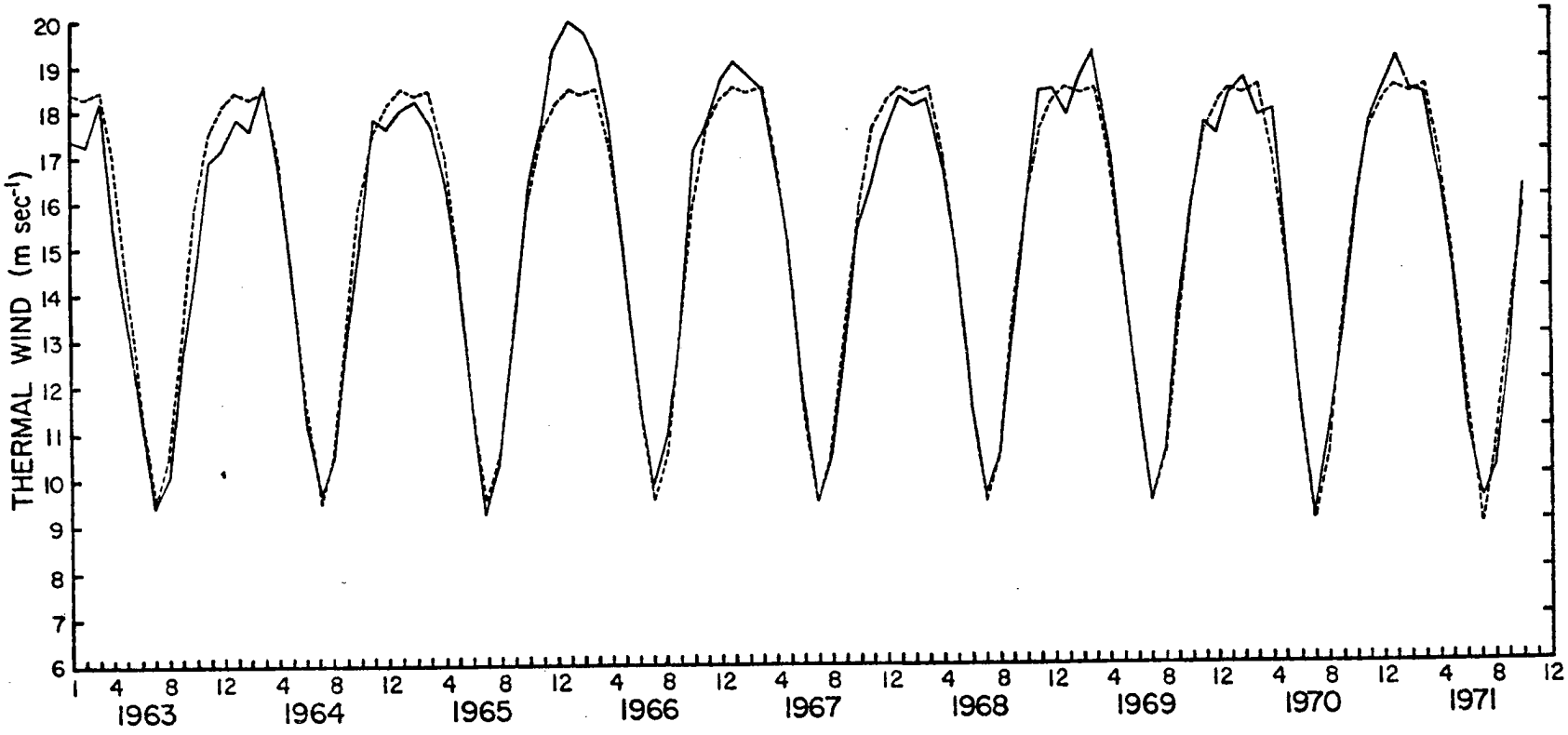

FIGURE 11. Northern hemisphere thermal wind for the layer 1000 mb to 300 mb from 20N to 90N (solid curve); mean monthly thermal wind based upon a 9 year average (dashed curve).

potential and kinetic energies which are partitioned into their zonal and eddy components one can observe the energy distribution between each component. A further refinement, which has not been done in this study, would be to compute the generation, conversion, and dissipation terms of the atmospheric energy cycle to see the actual mode of operation.

The relative distribution of energy between the zonal and eddy components is a function of the order used in computing space and time means. Oort (1964) discusses this thoroughly and establishes a set of equations for space, time, and mixed space-time domains. All computations in this study are within the mixed space-time domain. All integrations, taken over the mass of the atmosphere (trapezoidal method of integration was used), have limits from 850 to 200 mb and 20^{o}N to 90^{o}N. These limits were set because of data limitations in the NMC daily objective analysis. The zonal values were computed from the monthly mean data which included both the 00 and 12 GMT data. The eddy components were computed just from the daily 00 GMT data.

Symbology used in the equations is defined as follows:

p = pressure

p_o = 850 mb in this study

T = temperature in degrees absolute

m = mass

θ = potential temperature

u, v = east-west and north-south wind components

R = gas constant

C_p = specific heat at constant pressure

$[X]$ = zonal average of X

X^* = deviation from zonal average of X

$\overline{X}$ = time average of X

X' = deviation from time average of X

$\tilde{X}$ = area average of X over a closed isobaric surface

X'' = deviation from area average of X

3.3a Available Potential Energy

Zonal and eddy available potential energy are defined in the mixed space-time domain as:

$$P_m = \tfrac{1}{2} C_p \int \gamma \, [\overline{T}]''^2 \, dm \tag{7}$$

and

$$P_e = \tfrac{1}{2} C_p \int \gamma \, [\overline{T'^2} + \overline{T}^{*2}] \, dm, \tag{8}$$

respectively, with

$$\gamma = - \left(\frac{\theta}{\overline{T}} \right)^2 \frac{R}{C_p p_o} \int_0^{p_o} \left(\frac{T}{\theta} \right) \frac{1}{p} \left(\frac{\partial \tilde{\overline{\theta}}}{\partial p} \right) dp \tag{9}$$

Eq. (9) depends upon the mean static stability of the atmosphere; this is more apparent when γ is written in the form

$$\gamma = \frac{g}{C_p} (\Gamma_d - \overline{\Gamma})^{-1} \, \tilde{\overline{T}}^{-1}. \tag{10}$$

where Γ_d is the dry adiabatic lapse rate and $\overline{\Gamma}$ is the time mean lapse rate of the environment.

Eq. (9) can be used in the definition of available potential energy as:

$$\gamma = -k \left(\frac{\theta}{T} \right)^2 \tag{11}$$

where k is independent of pressure and time (Oort, 1964). The procedure used in this study was to compute k for each month of the 9 year period (106 values) and to use Eq. (11) in Eqs. (7 and 8).

Figures 12 and 13 show computed zonal (P_m) and eddy (P_e) available potential energies, respectively, for the 9 year period. Again, the dashed curve represents the average monthly values and does not change from year-to-year.

A large positive anomaly in P_m, approximately 12 percent of P_m, again appears in November 1965 through February 1966 as it had in the zonal index and thermal wind. Other anomalies that also appeared in the thermal wind are positive anomalies in January and February 1967, and February and April 1969, and a negative anomaly in winter 1967/68. As we shall see later, the mean available potential energy undergoes interannual variations in actual magnitude much larger than the three other energy terms.

The months for which radiation data were available (November 1965 and February and April, 1969) show corresponding variations in the net radiation gradient and P_m.

Eddy available potential energy shows instead of a positive departure from the mean in November 1965 through February 1966, a negative departure. Other features which stand out are the large positive departures in January 1963 and January through May 1967.

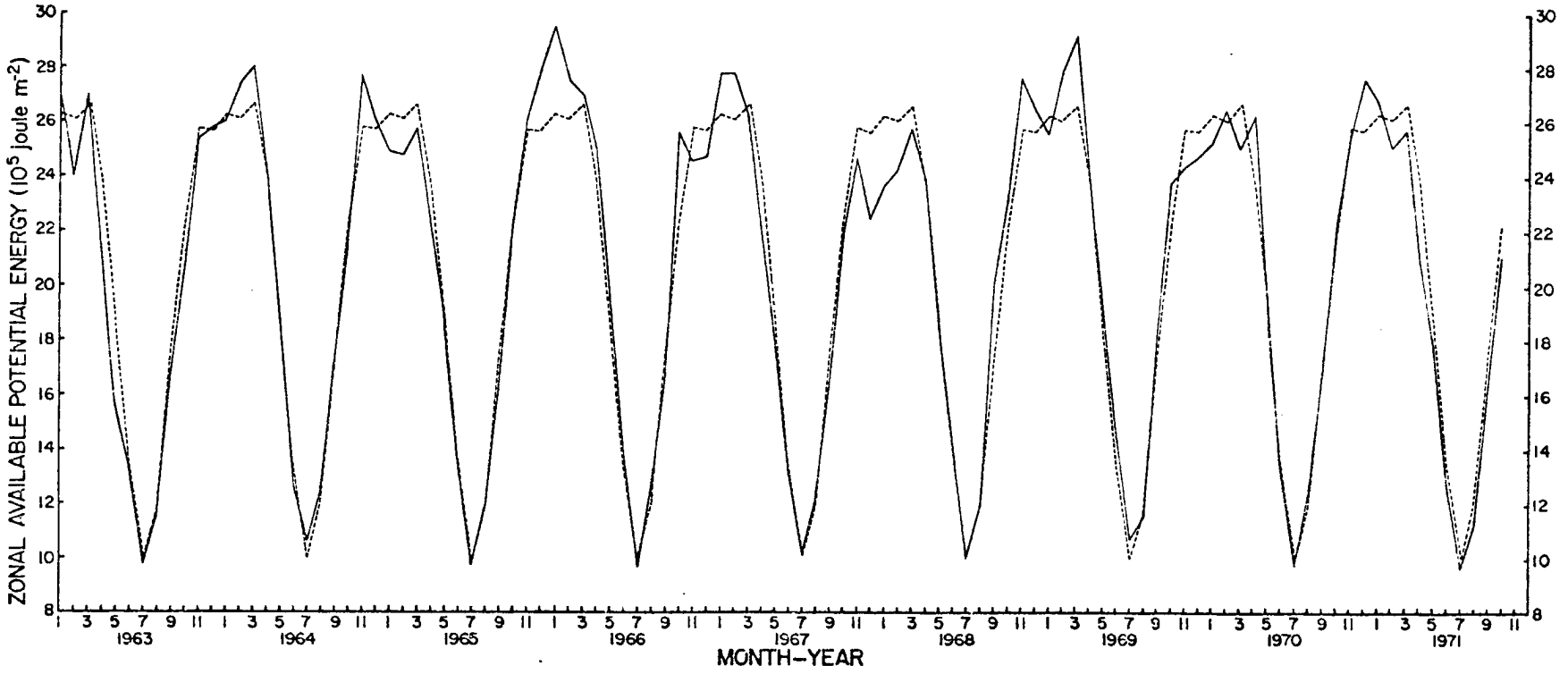

FIGURE 12. Northern hemisphere zonal available potential energy in the mixed space-time domain for the layer 850 mb to 200 mb fron 20N to 90N (solid curve); mean monthly zonal available potential energy based upon a 9 year average (dashed curve).

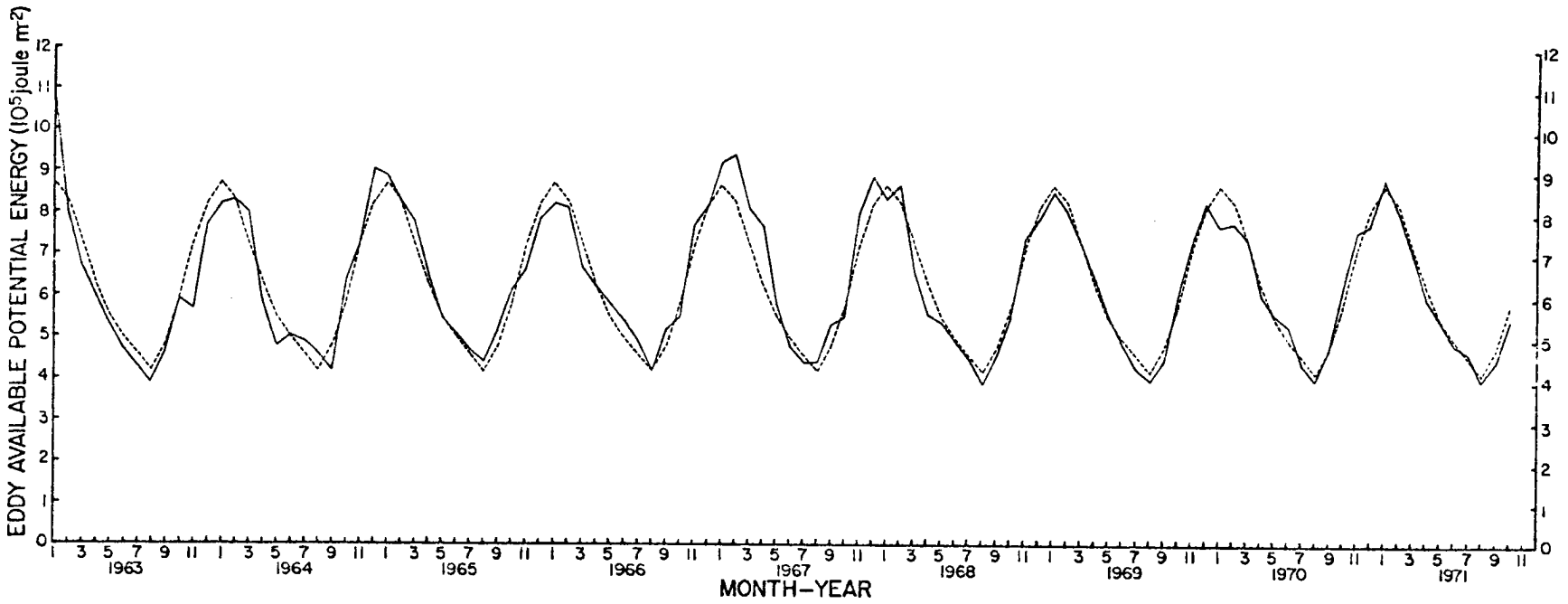

FIGURE 13. Northern hemisphere eddy available potential energy in the mixed space-time domain for the layer 850 mb to 200 mb from 20N to 90N (solid curve); mean monthly eddy available potential energy based upon a 9 year average (dashed curve).

However, no satellite data is available for these periods. The negative departure from November 1963 through January 1964 is in agreement with the net radiation gradient for the seasons SON 1963 and DJF 1963 (see Figure 3).

3.3b Kinetic Energy

Zonal and eddy kinetic energy are defined in the mixed space-time domain as:

$$K_m = \tfrac{1}{2} \int ([\bar{u}]^2 + [\bar{v}]^2)\, dm \qquad (12)$$

and

$$K_e = \tfrac{1}{2} \int [\overline{u'^2} + \overline{v'^2} + \bar{u}^{*2} + \bar{v}^{*2}]\, dm\ , \qquad (13)$$

respectively. Geostrophic winds were computed for this study since the actual winds in the NMC objective analysis were not available for the entire 9 year period. Because of the geostrophic approximation, the second term in Eq. (12) involving the zonal average of the meridional wind is zero. The latitudinal limits in the integration are also reduced to 22.5^{o}N and 87.5^{o}N.

The large positive anomaly which appeared in the other parameters for November 1965 through February 1966 again appears in Km (Fig. 14). The similarity of the interannual variations between Km and the other parameters stops here. Another striking feature, the largest anomaly in Km, is the large positive anomaly in January 1970. This anomaly in Km agrees with the large positive anomaly in the net radiation gradient in January 1970. Likewise, the negative anomaly in Km for November 1964 through February 1965 agrees with the negative anomaly in the gradient of net radiation for the same period.

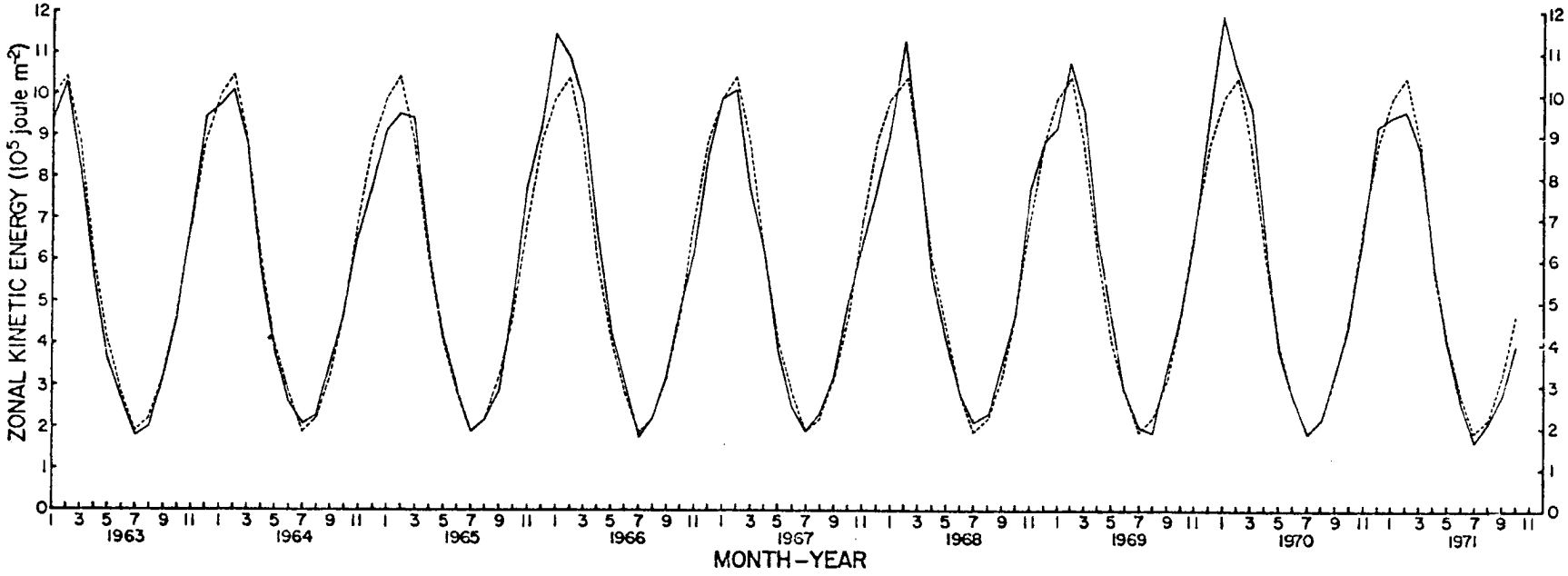

FIGURE 14. Northern hemisphere zonal kinetic energy in the mixed space-time domain for the layer 850 mb to 200 mb fron 20N to 90N (solid curve); mean monthly zonal kinetic energy based on a 9 year average (dashed curve).

The large positive anomaly in winter 1965/66 apparent in the other parameters is slightly negative in Ke (Fig. 15). Comparing Km and Ke one can conclude, to a first approximation, that the interannual variations in Km and Ke are inversely related. Of course this is an expected result; given a constant total kinetic energy, then an inverse relationship will exist between the mean and eddy components. This is a particular case which illustrates that given slight variations in impulse, the atmosphere may not respond with a change in its total energy but may only change its mode of energy transformation.

The foregoing qualitative discussion brought out that relationships between the interannual variations of the gradient and the general circulation parameters are apparent for the cases when variations in either one or both are very large. The relationship is summarized in Table 4. A positive sign indicates that the variations in the net radiation gradient and the general circulation parameters are of the same sign; a negative sign indicates that they are of opposite sign and a zero indicates that one of the variables does not deviate from the mean.

3.4 Quantitative Comparison

Correlation coefficients were computed between each of the general circulation parameters. The annual cycle was first removed from the data so that only interannual variations in the monthly values were compared. There were 106 samples of each parameter.

The results showed the best correlations of 0.68 and 0.67 between the thermal wind (V_T) and zonal available potential energy (Pm) and between eddy kinetic (Ke) and eddy potential energies (Pe),

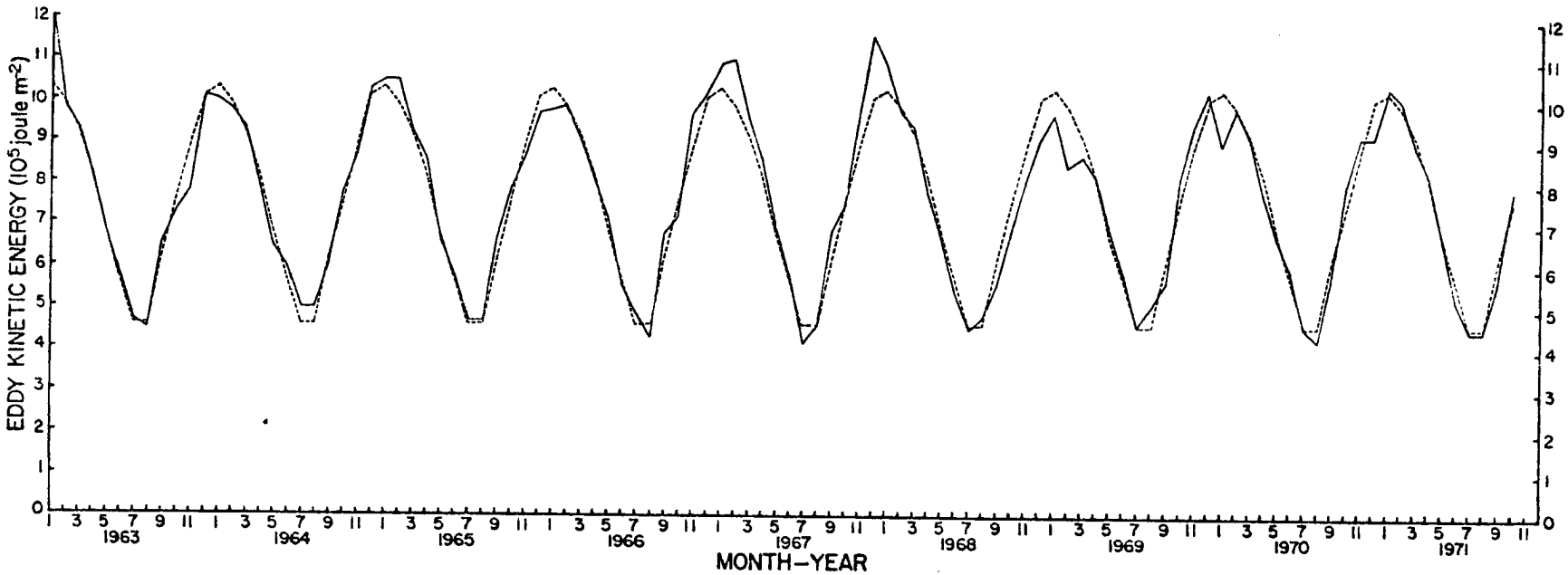

FIGURE 15. Northern hemisphere eddy kinetic energy in the mixed space-time domain for the later 850 mb to 200 mb from 20N to 90N (solid curve); mean monthly eddy kinetic energy based on a 9 year average (dashed curve).

TABLE 4: Summary table of qualitative comparison between interannual variations in the net radiation gradient and the general circulation parameters.

Parameter	J	F	M	A	M	J	J	A	S	O	N	D
ZI	-65 066 069 070	+65 -69	+65 -69	+65 +69	-65 +69	+65	065	+65	-65	+65	+65	066
V_t	+65 +69 -70	+65 +69	+65 +69	+69			+66			+65	+65 065	+64 066 +68
P_m	+65 -70	+65 +69	+65 +69	+65 +69			-64 069			+65 -68 +69	-64 +65 068	065 066 +68
P_e	-70									-65	-65	-64 -65
K_e	-65 069 -70	-65 -69	-69		-71		-64			-65 +68	-65 068	-68
K_m	+65 +70	+65								+65	+64 +65	+64

respectively. The high correlation between V_T and Pm is explainable in the fact that both parameters are a measure of the north to south atmospheric temperature difference. The large positive correlation between Ke and Pe is not so easily explained, but is directly dependent upon energy generation, dissipation and conversion rates. A correlation of -0.47 was found between the interannual variations of zonal kinetic and eddy kinetic energies which demonstrates to some degree the inverse relationship between the zonal and eddy components. A somewhat unexpected result was the lack of correlation between the interannual variations in the zonal kinetic energy and the zonal index. This again probably relates to the fact that the zonal index may be a better descriptor of the organization rather than the intensity of the general circulation.

Correlations coefficients were computed between the gradient of net radiation and the general circulation parameters with the annual cycle removed. The correlations were based on a sample size of 35 which require correlations larger than 0.335 and 0.430 to be significant at the 5 and 1 percent levels, respectively. The monthly means used to remove the annual cycle from the general circulation parameters were established from the same months which were used to remove the annual cycle from the net radiation gradient. In this respect, the interannual variations from both sets of data will be compared using input data from the same months.

The results are shown in Figures 16a and 16b. The computations were made with the net radiation gradient lagging the circulation parameters by 1 to 12 months (shown as a minus lag) and with circulation

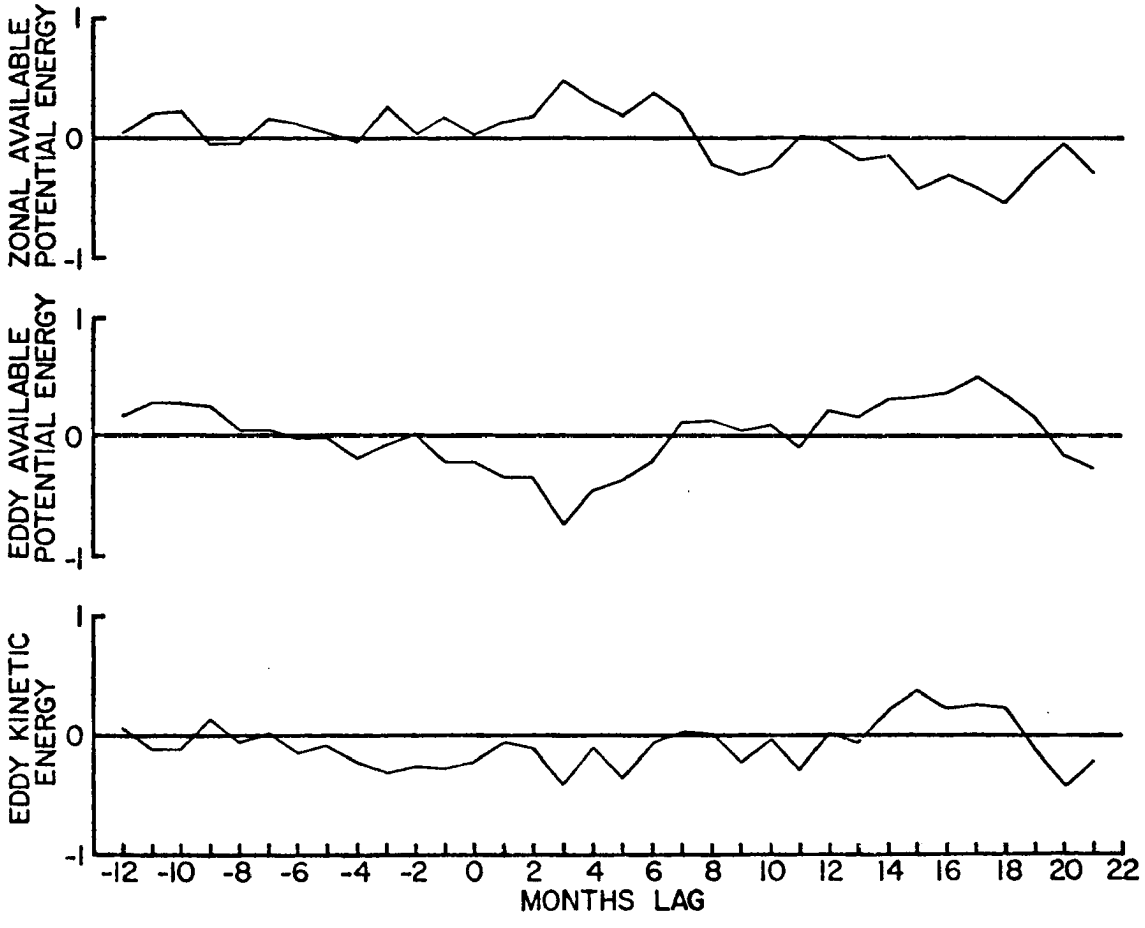

FIGURE 16a. Correlation coefficients of interannual variations with the general circulation parameters leading (-months) and lagging (+months) the net radiation gradient.

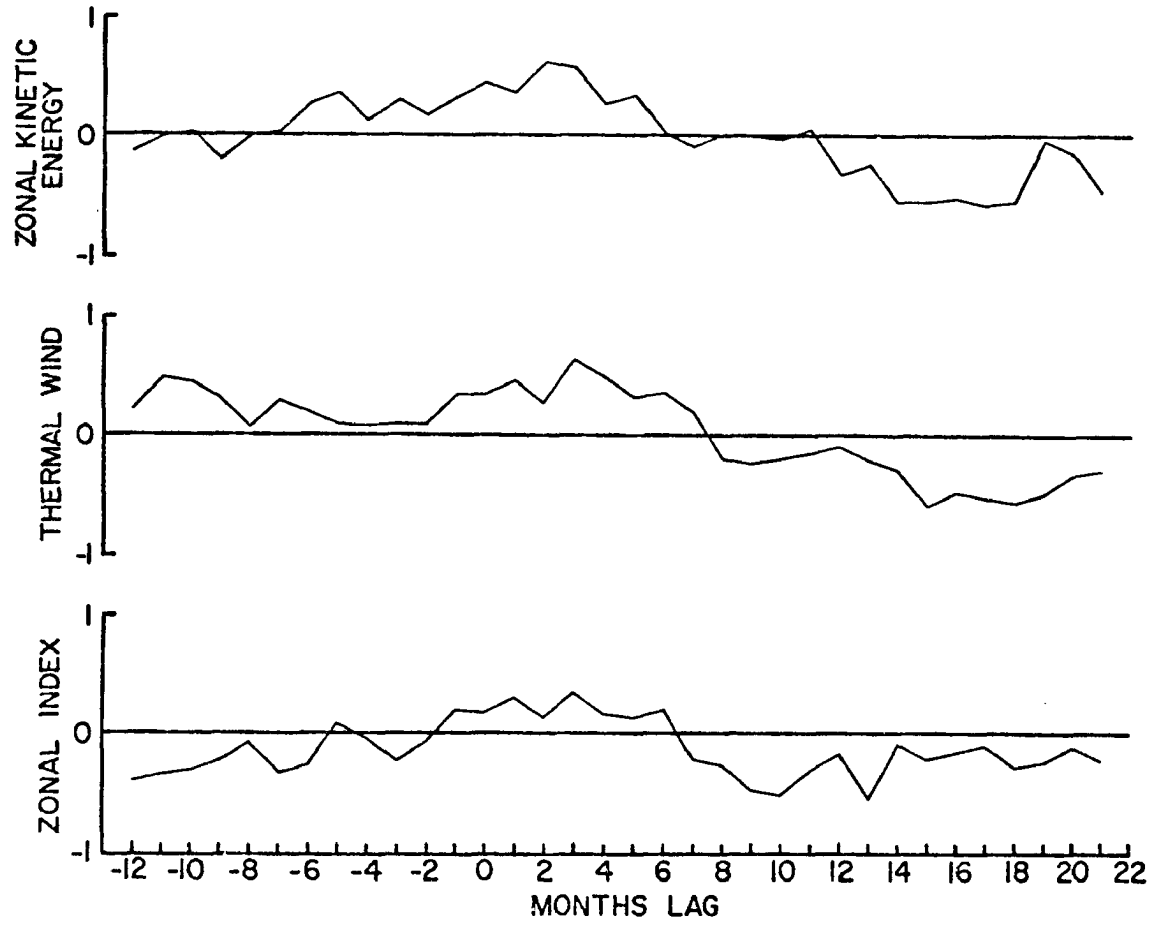

FIGURE 16b. Correlation coefficients of interannual variations with the general circulation parameters leading (-months) and lagging (+months) the net radiation gradient.

parameters lagging the net radiation gradient by 1 to 21 months (shown as a positive lag).

Excluding the zonal index, the best correlations appear with positive lags of 2 to 4 months. For the most part, these correlations are centered about a 3 month lag. Other correlations which are significant appear at 15 to 18 months lag with signs opposite of those at 3 months lag. These correlations have an average lag at 17 months.

Scanning the complete graph another general inflection in the curves appears at 9 to 10 months lead (-lag), especially prominent in the thermal wind and eddy potential energy. Going from crest to crest or trough to trough one sees that the wavelength is 26 to 27 months in length. Finding a wave in the correlations and especially a wavelength of 26 to 27 months was totally unexpected.

The lag relationship of the wave indicates that the general circulation parameters lead the net radiation gradient by 9 to 10 months or lag it by 3 months. Because of this wave, in contrast to the appearance of just one major peak in the correlation, no cause and effect relationship can be established.

Peak positive and negative correlations in the seasonal data were not as well defined--a most probable effect resulting from a smaller sample size (18) and averaging the data into seasonal values. For this reason, the interannual variations in the seasonal data will not be pursured any farther.

4.0 ANALYSIS OF RESULTS

4.1 Gradient and Circulation

Interannual variations in the net radiation gradient are indirectly caused by variations in the general circulation. Variations in the general circulation affecting the gradient are primarily manifested in cloudiness. For an example, decrease in middle and low cloudiness in the tropics contributes to a stronger north-to-south net radiation gradient.

Going one step farther, one should expect changes in the net radiation gradient to feed back into the general circulation. Knowing the time constant for the feedback may be important to long range weather prediction since the primitive equation models are presently limited to 10-14 day predictions.

It takes on the order of 4 to 6 weeks for the atmospheric temperature structure to respond to seasonal changes in the net radiation gradient as evidenced by the thermal wind lag. Also, there is an apparent 3 month response time between year-to-year differences in the net radiation gradient and the circulation parameters. Of course, this is based on an assumption that the two are related. In addition, there are a number of cases when a qualitative inspection showed that no apparent lag relationship existed between the year-to-year variations in the two.

A question to be answered is why the apparent cycle in correlations with a near 26 month period and why the initial 3 month lag in the circulation behind the gradient or, looking at it another way, why a 9 month lag in the gradient behind the general circulation.

4.1a Periodicity in Data

The cycle with approximately a 26 month period as seen in the correlation coefficients must result from a similar cycle in either one or both of the data sets used in the correlation.

With some imagination, one can fit a sine curve with approximately a 26 month period to a time series of the interannual variations in the monthly net radiation gradient ($\Delta RN'$) (Fig. 17). A definite increase is apparent in $\Delta RN'$ from early fall 1964 to winter 1965/66. This same general trend, but not as well defined, appears in early fall 1968 to the latter part of 1969 and is just two wavelengths downstream from the earlier trend. Therefore, the $\Delta RN'$ data will tend to correlate with any other data set which contains a 26 month period when certain lags are introduced.

Could this cycle be indicative of the 26 month or quasi-biennial cycle? The temporal distribution of $\Delta RN'$ did not definitely show the cycle but indicated that one may be present. Data is needed in 1967 and early 1968 so that, at least, the existence of one wave might be verified. Future measurements by satellites will enable us to draw valid conclusions concerning the presence of a 26 month oscillation in the data.

If the quasi-biennial cycle is in $\Delta RN'$, then it is most likely in the interannual variations in tropospheric cloudiness since cloudiness is the primary modifier of $\Delta RN'$. That it is in the tropospheric cloudiness is supported by the fact that it has been found in the temporal distribution of tropical precipitation (Garstang, 1967).

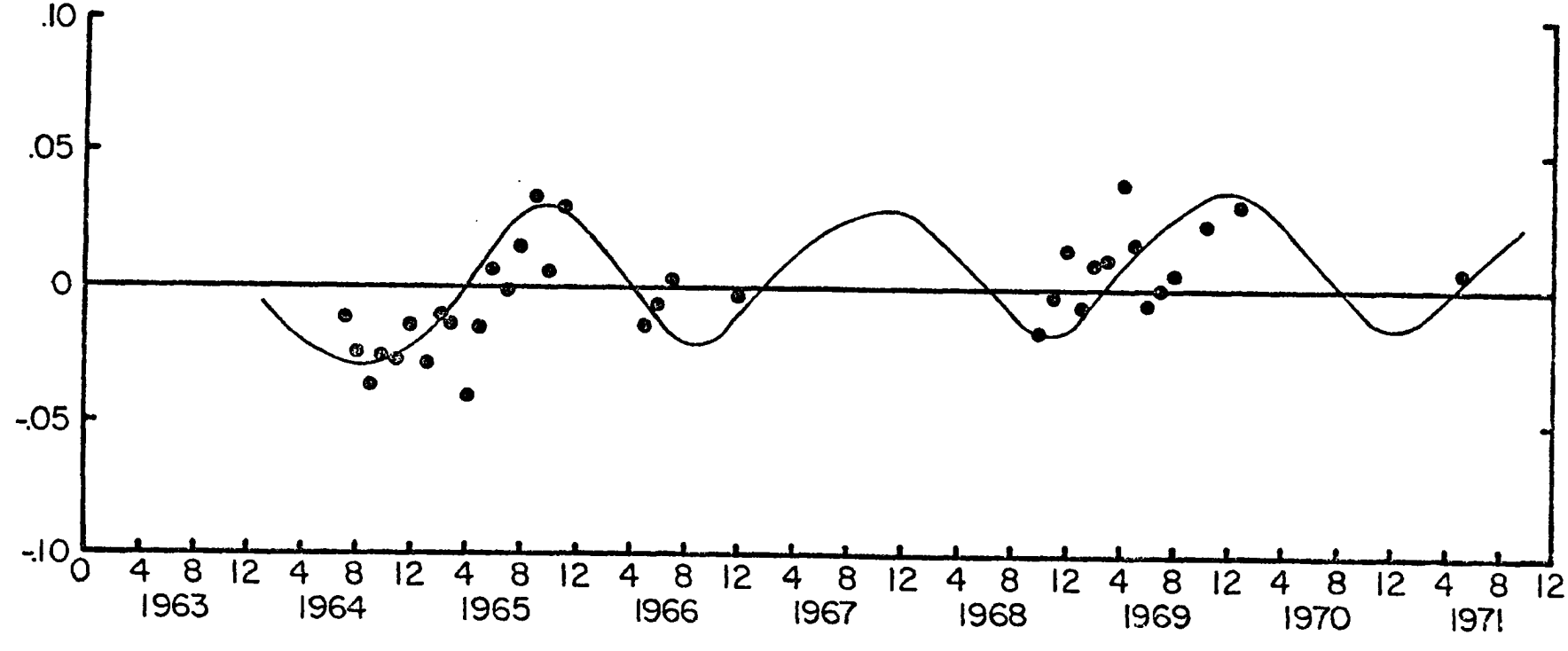

FIGURE 17. Temporal distribution of the net radiation gradient with the annual cycle removed (ΔRN').

A wave with a 26 month period must exist in the general circulation parameters since no well defined wave was found in the $\Delta RN'$. Such periodicity has been found in the mid-latitude troposphere by investigation of the sea level zonal index (Brier, 1969), in surface temperature (Landsberg et al., 1963), and 500 mb angular momentum transport (Miller, et al., 1967). Many studies indicate a dominating role of winter months in the 26 month oscillation (see Reiter, 1969).

To determine if such a wave exists in the general circulation data with the annual cycle removed--which was intercompared with the satellite measurements--a power spectrum analysis was performed on each 9 year data set. The first 11 harmonics representing periods of 108 months to 9.8 months are shown in Figure 18. One would expect to see a relatively large percent variance for the fourth harmonic (27 months period) if the quasi-biennial oscillation is in the data. Indeed, such large variance is seen in the smoothed spectrum (solid curve) for eddy available potential energy--the same parameter which had the most distinguishable 26 month cycle in the correlation coefficients (Fig. 16a). The smoothed spectrum does not show the 27 month periodicity nearly as well in the other parameters. However, the unsmoothed spectrum (dashed) shows a peak in the variance at 27 months periodicity in all parameters but the zonal index and zonal kinetic energy. The predominate variance in zonal kinetic energy and the thermal wind is with a periodicity on the order of 54 months rather than 27 months. In all, the two eddy parameters show a 27 month periodicity best.

The spectrum for zonal kinetic energy shows a minimum of variance at 27 months but the correlation coefficients showed a well

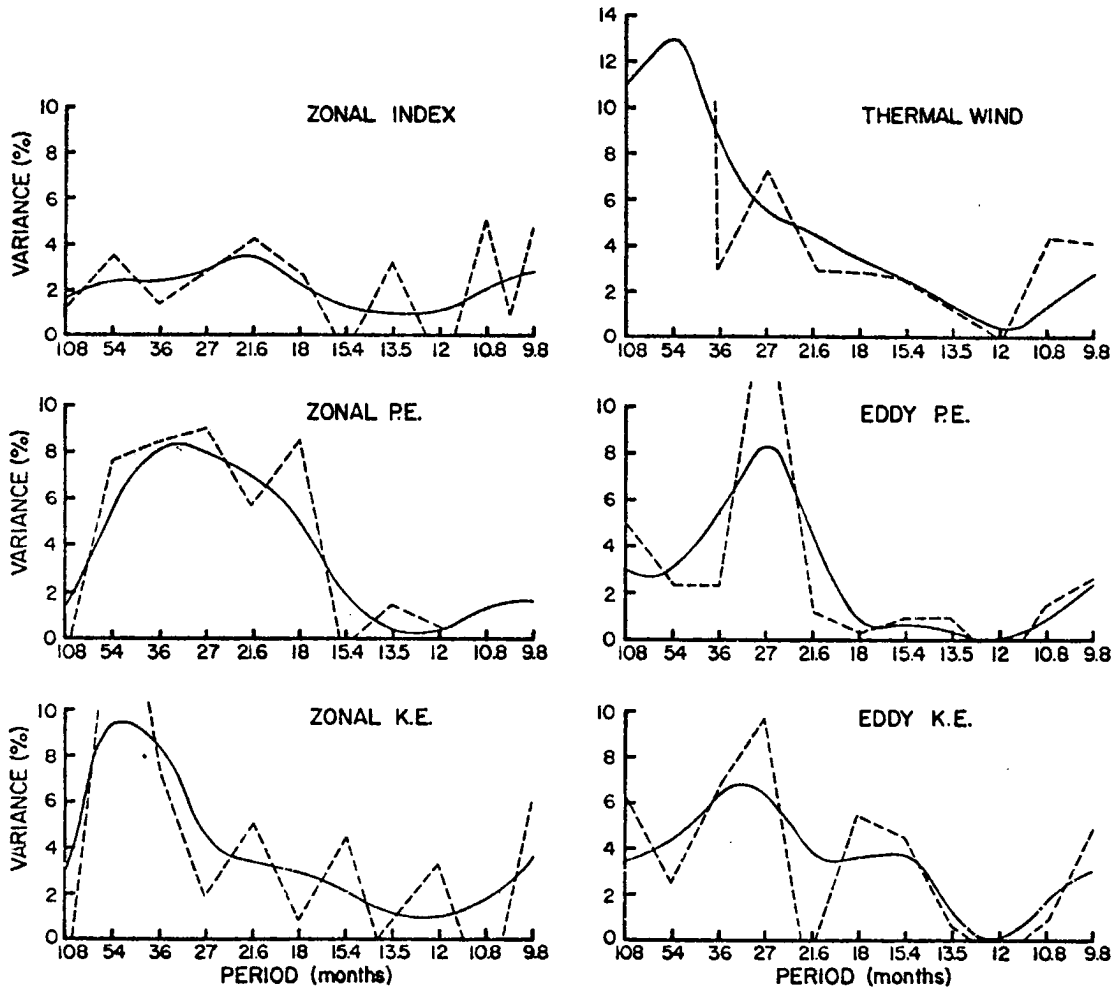

FIGURE 18. Spectrum analysis of general circulation parameters: smoothed spectrum (solid line), unsmoothed spectrum (dashed line).

defined half wavelength from 3 months to 16 months lag. Therefore, it appears that a 26 month oscillation exists in the satellite measurements.

4.1b 3 Month Lag

The next question to be investigated is the 3 month lag in the correlations--a feature common to all general circulation parameters. The phase relationship between ocean storage and the atmospheric circulation might be the best place to look.[1] The seasonal storage curves for the northern hemisphere at latitudes 5N, 30N, and 65N show in the periods March-April and September-October, no net energy transfer between oceans and atmosphere (Fig. 19). If the oceanic storage is the primary agent contributing to a 3 month lag, then, during these periods, no large lag relationship should exist.

Examination of the month to month correlations between interannual variations in zonal available potential energy (P_m) and the net radiation gradient (RN) with both no lag and a 3 month lag might give evidence of the oceanic influence (Fig. 20). The solid bars represent interannual variations in ΔRN while the other bars represent the same variations in P_m . In the period March-April the correlations are nearly as good with and without a lag relationship except that the no lag may be slightly better. The ΔRN' for March, along with the period May through July (except July, 1966)

[1]Professor Verner E. Suomi originally suggested this line of inquiry.

defined half wavelength from 3 months to 16 months lag. Therefore, it appears that a 26 month oscillation exists in the satellite measurements.

4.1b 3 Month Lag

The next question to be investigated is the 3 month lag in the correlations--a feature common to all general circulation parameters. The phase relationship between ocean storage and the atmospheric circulation might be the best place to look.[1] The seasonal storage curves for the northern hemisphere at latitudes 5N, 30N, and 65N show in the periods March-April and September-October, no net energy transfer between oceans and atmosphere (Fig. 19). If the oceanic storage is the primary agent contributing to a 3 month lag, then, during these periods, no large lag relationship should exist.

Examination of the month to month correlations between interannual variations in zonal available potential energy (P_m) and the net radiation gradient (RN) with both no lag and a 3 month lag might give evidence of the oceanic influence (Fig. 20). The solid bars represent interannual variations in ΔRN while the other bars represent the same variations in P_m . In the period March-April the correlations are nearly as good with and without a lag relationship except that the no lag may be slightly better. The ΔRN' for March, along with the period May through July (except July, 1966)

[1]Professor Verner E. Suomi originally suggested this line of inquiry.

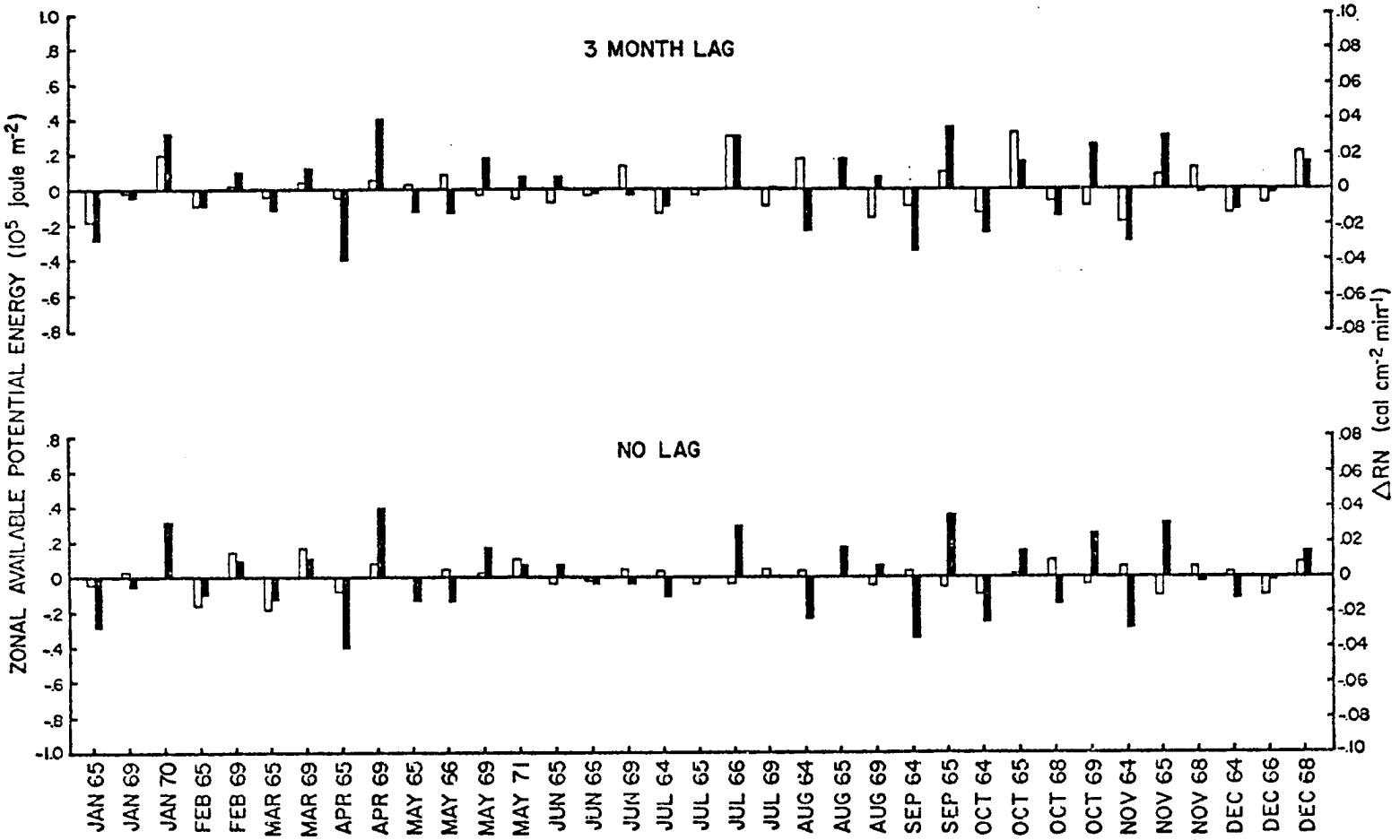

FIGURE 20. Correlation between interannual variations in net radiation gradient (black bars) and zonal available potential energy (light bars) with 3 months lag and no lag.

are within or are very near the bias error of ± 0.01 cal cm^{-2} min^{-1} (see section 2.3a) and, therefore, may not be relevant. Looking at the period, September-October, all but one sample shows positive correlation with a 3 month lag and all but one sample shows a negative correlation with no lag--a reverse relationship from what would be expected with the atmosphere-oceans decoupled (no lag) and coupled (3 month lag). Hence, the oceanic storage effect on the lag as hypothesized is not strongly apparent in the correlations.

Correlations are best when interannual variations in ΔRN and the circulation parameters are anomalously large in the same direction. Examination of the interannual variations in ΔRN and zonal kinetic energy with 3 month lag (Fig. 21) reveals a grouping of large anomalous $\Delta RN'$ in the fall pairing up with large anomolous zonal kinetic energy in winter. This same grouping is apparent, but to a lesser extent, with the other circulation parameters (inverse relationship with the eddy parameters). Therefore, it appears that the fall-winter relationship in the correlations is the prime contributor to the 3 month lag.

4.2 Interhemisphere Comparison

The $\Delta RN'$ for the northern hemisphere (solid line) are compared to the $\Delta RN'$ for the southern hemisphere (Fig. 22). All $\Delta RN'$ greater than the maximum bias error of ± 0.014 cal cm^{-2} min^{-1} are in phase between hemispheres except for the January months. The January 1970 irregularity is primarily contributed to by the January 1970 gradient anomaly; January 1970 was the month with a very large positive anomaly in the zonal kinetic energy.

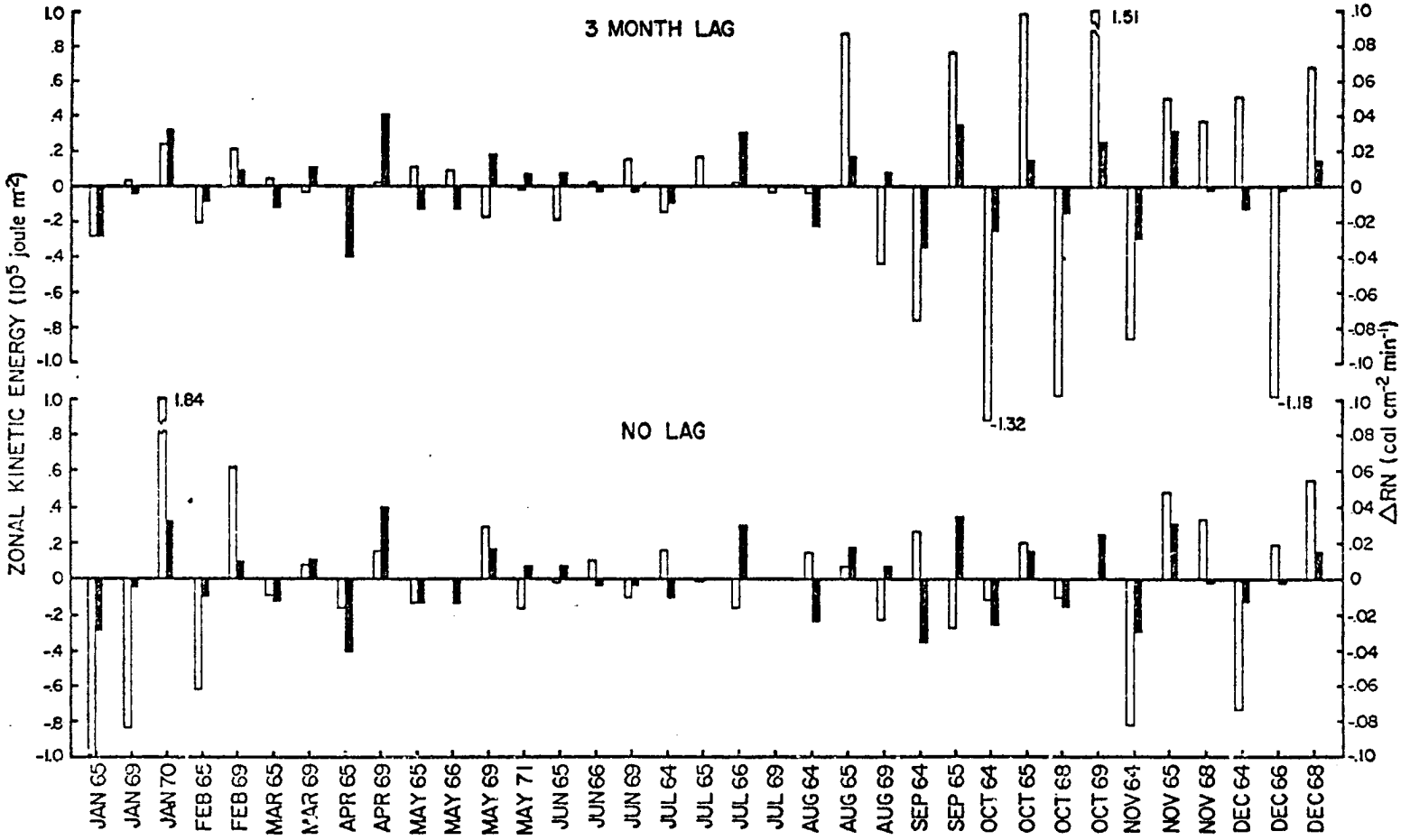

FIGURE 21. Correlations between interannual variations in net radiation gradient (black bars) and zonal kinetic energy (light bars) with 3 months lag and no lag.

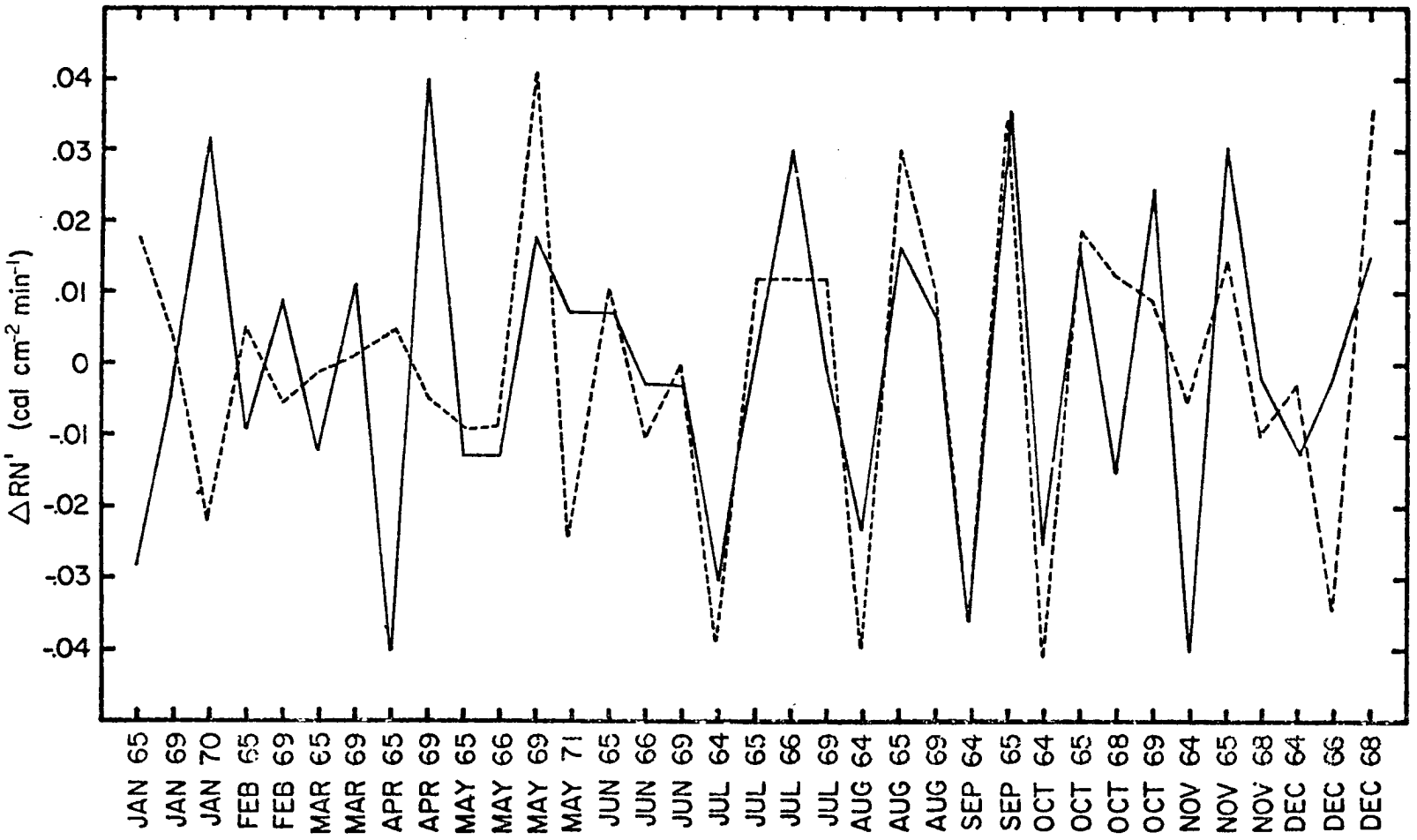

FIGURE 22. Temporal comparison between interannual variations in the net radiation gradient of the northern hemisphere (solid line) and the southern hemisphere (dashed line).

The in phase relationship appearing in the months of June through December implies either one or both of the following: (1) the net radiation budget of the tropical region, which is common to both hemispheres, is undergoing large year to year changes, or (2) the net radiation budget of both the north and south near polar regions are changing year to year with the same sign. The first of these possibilities is the most logical choice. However the cause cannot be isolated until all radiation data are normalized to eliminate the diurnal variation between data sets.

Regardless of the cause, the $\Delta RN'$ are in general, simultaneously large or small in both hemispheres. If a true relationship exists between $\Delta RN'$ and the general circulation, then one should expect to see a relationship in the year to year variations of the general circulation parameters between each hemisphere. An analysis of the general circulation of the southern hemisphere is needed to confirm such related variations.

4.3 Gradient and Cloudiness

A particular case, April 1965 compared to April 1969, has been selected for study. These two months comprised the strongest inter-annual variation in ΔRN for all the data sets. Allison et al. (1971) found minimum and maximum cloudiness in the eastern tropical Pacific for April 1965 and April 1969, respectively. The zonal averages of albedo were higher in April 1969 (25 percent) than in April 1965 (22 percent). These albedoes were reflected in the net radiation budget at 5N as 0.12 cal cm^{-2} min^{-1} for April 1969 and as 0.15 cal cm^{-2} min^{-1} for April 1965. Therefore, a stronger north-to-south

net radiation gradient would prevail with the less tropical cloudiness period of April 1965.

However, overcompensating changes took place at 65N so that the gradient was much stronger in the more tropical cloudiness period of April 1969. The change from April 1965 to April 1969 at 65N was an increase in both the albedo and longwave loss from 37 to 52 percent and 0.24 to 0.29 cal cm^{-2} min^{-1}, respectively; thus, changing the radiation budget from 0.01 to -0.10 cal cm^{-2} min^{-1}. These changes in the later period (1969) could be indicative of above normal low and middle cloudiness at 65N.

For this particular case, changes in the near polar region had a greater effect on the gradient than the apparent extreme change in cloudiness in the tropical regions. All general circulation parameters relate positively to the April 1965 and April 1969 change in ΔRN (except for the eddy components which show inverse relationship) for both no lag and 3 month lags. The zonal index and zonal kinetic energy show a preference for a stronger postive relationship with no lag. Hence, the interannual variations in both ΔRN and general circulation parameters appear to be related in this particular case. So here is a case exemplifying the need for study in the near polar regions for a better understanding of anomalies in the atmosphere.

5.0 SUMMARY AND CONCLUSIONS

The pole to equator gradient of net radiation and the general circulation of the atmosphere were brought together in an interrelated study for the first time. Interannual variations in the gradient of net radiation and the intensity of the general circulation appear to be related.

In most cases when variations in the net radiation gradient were large, corresponding large anomalies were found in one or more of the general circulation parameters. However, the study was not restricted to extreme cases.

Statistical correlations between the gradient of net radiation and each of the general circulation parameters, with the annual cycle removed from each variable, were best when the general circulation parameters lagged the net radiation gradient by 3 months. Eddy available potential energy showed the best correlation at -0.73 followed by the thermal wind, zonal kinetic energy, zonal available potential energy, and eddy kinetic energy at +0.64, +0.56, +0.49, and -0.38, respectively. Statistical significant correlations were found at 16 to 18 months lag in all the circulation parameters but with an inverse sign from those at 3 months lag. A similar inverse trend appeared with a lead of 9 to 11 months. All correlations taken together show a wave with a wavelength of 26 to 27 months which is either 3 months or 9 to 10 months out of phase with the net radiation gradient. Additional satellite data are needed to ascertain the validity of this wave and the phase relationship.

This type of gradient can be obtained on a routine basis as satellite data becomes available. Providing these results continue to bear out, then such statistics will be a step forward towards the prediction of the general circulation on monthly and seasonal basis, a hurdle yet to be surmounted by the primitive equation models.

Future studies should investigate in more depth the role of cloudiness in the gradient of net radiation, and the feedback mechanisms relating the net radiation gradient, cloudiness, and the intensity of the general circulation.

REFERENCES

Allison, L. J., J. Steranka, R. J. Holub, J. Hansen, F. A. Godshall, and C. Prabhakara, 1971: Air sea interaction in the tropical Pacific ocean. U. S. Dept. of Commerce N71-27648.

Brier, G. W., 1969: Long range weather prediction of the zonal westerlies and some problems in data analysis. Rev. Geoph., 6, 4, pp. 525-551.

Garstang, M. and T. R. Visvanathan, 1967: Solar and lunar influences on rainfall. Department of Meteorology, Florida State Univ., Tallahassee, Florida.

Kutzback, J. E., R. A. Bryson, and W. C. Shen, 1968: An evaluation of the thermal Rossby number in the Pleistocene, Met. Mono., 8, 30, pp. 134-138.

Landsberg, H. E., J. M. Mitchell, Jr., H. L. Crutcher and J. T. Quinlan, 1963: Surface signs of the biennial atmospheric pulse. Mon. Wea. Rev., 91, 10-12, pp. 549-556.

MacDonald, T. H., 1969: Private communication.

MacDonald, T. H., 1970: Data reduction processes for spinning flat-plate satellite-borne radiometers. ESSA Tech. Report NESC 52.

MacDonald, T. H., 1972: Private communications.

Miller, A. J., S. Teweles, and H. M. Woolf, 1967: Quasi-biennial cycles in angular momentum transports at 500 mb. Jour. Atmos. Sci., 24, 3, pp. 298-304.

Namias, J., 1950: The index cycle and its role in the general circulation. Jour. of Met., 7, 2, pp. 130-139.

Newell, R. E., D. G. Vincent, T. G. Dopplick, D. Ferruzza, and J. W. Kidson, 1969: The energy balance of the global atmosphere. AMS-RMS Joint Conference on Global Circulation of the Atmosphere, London, England.

Oort, A. H., 1964: On estimates of the atmospheric energy cycle. Mon. Wea. Rev., 92, 11, pp. 483-493.

Raschke, E., 1968: The radiation balance of the earth-atmosphere system from radiation measurements of the Nimbus II meteorological satellite. NASA TN D-4589.

Raschke, E. and W. R. Bandeen, 1970: The radiation balance of the planet earth from radiation measurements of the satellite Nimbus 2. Jour. Appl. Met., 9, 2, pp. 215-238.